JOURNAL OF GEOPHYSICAL RESEARCH, VOL. 106, NO. D8, PAGES 7857–7878, APRIL 27, 2001

Climatological characteristics of the tropical tropopause as revealed by radiosondes

Dian J. Seidel, Rebecca J. Ross, and James K. Angell
NOAA Air Resources Laboratory, Silver Spring, Maryland

George C. Reid
Cooperative Institute for Research in Environmental Sciences, University of Colorado, Boulder, Colorado

Abstract. A temporally and spatially comprehensive depiction of the tropical tropopause is presented, based on radiosonde data from 83 stations. Climatological statistics for 1961–1990 are computed for three levels: the conventional lapse-rate tropopause (LRT), the cold-point tropopause (CPT), and the 100 hPa level. Mean values and seasonal and interannual variations of temperature, pressure, height, potential temperature, and water vapor saturation mixing ratio at these levels are compared. The tropopause is higher, colder, and at lower pressure in the Northern Hemisphere (NH) than in the Southern Hemisphere (SH) in NH winter. This pattern reverses in NH summer, except that the tropopause remains colder in the NH than in the SH. The climatological locations of minimum tropopause temperature differ from those of maximum height and minimum pressure: In NH winter the tropopause is coldest over the western tropical Pacific warm pool region, but it is highest and at lowest pressure over the western Atlantic. Correlations of interannual anomalies in zonal-mean characteristics reveal that the height of the tropopause reflects the temperature of the underlying troposphere. Tropopause temperature, on the other hand, shows little association with tropospheric characteristics but is significantly correlated with the temperature and pressure of the lower stratosphere. The 100 hPa level is a poor surrogate for the tropical tropopause. Changes in radiosonde instrumentation limit the potential for detecting tropopause trends. However, the following (nonmonotonic) trends in the tropopause in the deep tropics during 1978–1997 seem robust: an increase in height of about 20 m decade^{-1}, a decrease in pressure of about 0.5 hPa decade^{-1}, a cooling of about 0.5 K decade^{-1}, little change in potential temperature, and a decrease in saturation volume mixing ratio of about 0.3 ppmv decade^{-1}.

1. Introduction

Atmospheric scientists have known of the existence of the tropopause for nearly a century. The surprising discovery of a temperature inversion layer 10–15 km above the surface in midlatitudes was the result of careful, repeated observations by Léon Teisserenc de Bort, in France, and Richard Assman, in Germany, both using instruments carried aloft by balloons. *Ohring* [1964] and *Hoinka* [1997] recount details of these turn-of-the-century observations. It was not until midcentury, however, with the expansion and improvement of the radiosonde network for the International Geophysical Year (1957–1958), that routine measurements of the tropopause became available. At that time, a formal definition of the tropopause was adopted by the World Meteorological Organization as "the lowest level at which the lapse rate decreases to 2°C/km or less, provided also the average lapse rate between this level and all higher levels within 2 km does not exceed 2°C/km" [*WMO*, 1957].

This thermal definition of the tropopause, based on lapse rate, is most appropriate for the tropics. In middle and high latitudes a discontinuity in potential vorticity is more commonly used to define the tropopause, separating low tropospheric values from high stratospheric values [e.g., *Reed*, 1955; *Hoinka*, 1997]. Identifying the dynamical tropopause involves evaluating horizontal gradients of the wind field from upper air analyses. The thermal tropopause, on the other hand, can be identified locally using temperature-sounding data alone, an advantage in data-sparse regions, such as the tropics. In this paper we will refer to the tropopause identified using the formal, lapse-rate definition as the lapse-rate tropopause (LRT). A second thermal definition of the tropopause is the location of the coldest point in the temperature sounding, which we will refer to as the cold-point tropopause (CPT). This definition is preferred in studies of the cross-tropopause flux of water vapor in the tropics.

Recently, scientific attention to the roles of the stratosphere in the climate system [*Brasseur*, 1997] has sparked renewed interest in the tropopause, particularly in the tropics [*Highwood and Hoskins*, 1998]. The transport of water vapor and other trace constituents through the tropical tropopause affects their concentration and distribution in the stratosphere [*Mote et al.*, 1996; *Dessler*, 1998]. Long-term changes in the characteristics of the tropical tropopause may be associated with changes in stratospheric water vapor concentrations [*Angell and Korshover*, 1976; *Frederick and Douglass*, 1983]. Because increases in stratospheric water vapor, as demonstrated

Paper number 2000JD900837.
0148-0227/01/2000JD900837$09.00

by balloon-borne frost-point hygrometer observations [*Oltmans and Hofmann*, 1995], have been postulated as playing a role in cooling the lower stratosphere [*Forster and Shine*, 1999] and depletion of ozone in the Arctic stratosphere [*Kirk-Davidoff et al*., 1999], a better understanding of tropical tropopause changes could clarify the causes of global and regional temperature and stratospheric ozone trends.

At least in midlatitudes, both total column ozone abundance and tropospheric temperature are correlated with tropopause height [*Steinbrecht et al*., 1998], and it seems reasonable that similar relationships may hold in the tropics. Annual and interannual variations in the height of the tropical tropopause are correlated with atmospheric angular momentum [*Reid and Gage*, 1984], a fundamental aspect of the global atmospheric circulation. Thus understanding variations in the tropical tropopause can provide insight into a range of issues related to global atmospheric chemistry and climate.

Most previous observational studies of the tropical tropopause have relied on radiosonde data. A series of extensive analyses of the long-term records from a handful of radiosonde stations, mainly in the western tropical Pacific region, has shed light on the physical processes that control seasonal and interannual variations in the tropical tropopause. The annual cycle has been linked to seasonal variations in solar radiation and its impact on tropical convection [*Reid and Gage*, 1981; *Shimizu and Tsuda*, 2000] and to remote forcing during boreal winter associated with the intensification of the Brewer-Dobson circulation [*Reid and Gage*, 1996]. Interannual variations in the tropical tropopause have been linked to the quasi-biennial oscillation of the equatorial stratosphere [*Angell and Korshover*, 1964, 1974; *Reid and Gage*, 1985], the El Niño-Southern Oscillation [*Gage and Reid*, 1985, 1987], and episodic volcanic eruptions [*Reid and Gage*, 1985].

The passage of half a century since the main expansion of the radiosonde network, and the availability of new aerological data sets, afford the opportunity to develop a more temporally and spatially comprehensive depiction of the tropopause than ever before. This paper exploits these facts in exploring a suite of various climatological features of the tropical tropopause. This study is based exclusively on radiosonde data, but it is worth noting the existence, utility, and potential disadvantages of atmospheric reanalysis products for this same purpose.

Assimilating observational data into a global numerical weather prediction model results in spatially complete and dynamically consistent atmospheric analyses. Such assimilations, performed using a fixed, state-of-the-art model to analyze archived observations for long periods of record, yield "reanalyses" that do not suffer from time-varying biases associated with changes in the operational numerical model [*Kalnay et al*., 1996; *Gibson et al*., 1997]. In the past few years, such analyses and reanalyses have been used in studies of the tropopause. *Highwood and Hoskins* [1998] employed European Centre for Medium-Range Weather Forecasts (ECMWF) analyses for a 4 year period (1991–1995), along with monthly mean radiosonde data, to study the tropical tropopause. *Hoinka* [1998, 1999] used ECMWF reanalysis data for 1979–1993 to study the pressure [*Hoinka*, 1998], temperature, humidity, and wind [*Hoinka*, 1999] at the tropopause globally. *Randel et al*. [2000] compared tropical tropopause temperature and pressure values from the National Centers for Environmental Prediction (NCEP) reanalyses with radiosonde observations and found systematic high biases in both temperature and pressure, as well as evidence of abrupt, and probably artificial, jumps in tropopause characteristics around 1978 when satellite data were first available for assimilation into the reanalysis. Despite these issues, the NCEP reanalysis data yield reasonable information on seasonal and interannual variations in the tropical tropopause. In each of these studies, the tropopause was defined as the LRT, although *Hoinka* [1998, 1999] also used the dynamical definition, based on potential vorticity. Examining the variability of the tropical CPT, *Zhou et al*. [2000a] identified systematic temperature and pressure biases in the ECMWF reanalysis CPT compared with radiosonde data, similar to those found in the NCEP reanalysis data by *Randel et al*. [2000].

The temporal inhomogeneity in the tropopause as depicted in the NCEP reanalysis is an example of one potential disadvantage for the use of reanalysis products in studies of long-term change. A second drawback of both analyses and reanalyses is the limited vertical resolution of the models in the tropopause region. The vertical resolution of the ECMWF reanalysis is 20 hPa near the 100 hPa level according to *Hoinka* [1998], although *Zhou et al*. [2000a] report a coarser resolution, and that of the NCEP reanalysis is about 2 km (20–30 hPa) [*Randel et al*., 2000]. The precision of the identification of the tropopause from the reanalyses is thus limited by the model resolution, which may explain, in part, why maps of the tropical tropopause based on (re)analyses show limited spatial structure [*Hoinka*, 1998; *Highwood and Hoskins*, 1998].

In contrast, radiosonde observations are supposed to include data at "significant levels," where the observations between mandatory reporting levels depart from a linear interpolation, such as would occur at the tropopause. In recent decades a tropopause level report has been explicitly required. Monthly mean radiosonde data, such as were employed by *Highwood and Hoskins* [1998], and by *Parker et al*. [1997] in their long-term temperature data set, are limited to the mandatory levels. The mandatory levels near the tropical tropopause are 150, 100, 70, and 50 hPa. Thus daily radiosonde data offer considerably better vertical resolution near the tropopause than either monthly radiosonde data or (re)analyses. Furthermore, the use of daily soundings eliminates biases associated with using monthly data to vertically interpolate the tropopause level and to calculate variables, such as water vapor saturation mixing ratios, which are nonlinearly related to observed temperature and heights at fixed pressure levels [*Frederick and Douglass*, 1983; *Highwood and Hoskins*, 1998; *Dessler*, 1998].

In this paper we use a 30 year radiosonde data set to explore the climatological characteristics of the tropical tropopause. Section 2 discusses the observations and their processing. Section 3 presents a comprehensive discussion of the characteristics of the lapse-rate tropopause, cold-point tropopause, and the 100 hPa level, including tropopause height, pressure, temperature, saturation volume mixing ratio of water vapor, and potential temperature. Section 4 examines the interannual variability of the tropopause, including correlations with the troposphere and stratosphere and long-term trends. Section 5 summarizes our main findings.

2. Radiosonde Data

Radiosonde data are available from several sources, but the most complete archive is probably the Comprehensive Aerological Reference Data Set [*Eskridge et al*., 1995], which is the source of observations for this study. We employ data from 108 radiosonde locations in the tropical belt (30°N–30°S) in a subset of stations identified by *Wallis* [1998] as a "core" network,

with good spatial and temporal coverage. The focus of this study is climatological fields for the most recent climatic normal period 1961–1990, although the complete data record at some stations spans 1948–1997, and we employ data through 1997 in section 4.

2.1. Individual Soundings

From each sounding, we locate the following five levels relevant to the study of the tropical tropopause: (1) the lapse-rate tropopause (LRT) based on the *WMO* [1957] definition; (2) the cold-point tropopause (CPT) based on the minimum temperature of the sounding; (3) the 100 hPa level, which is sometimes used as a surrogate for the tropical tropopause [*Frederick and Douglass*, 1983; *Mote et al*., 1996]; (4) the level at which water vapor saturation volume mixing ratio with respect to ice (q_s) reaches a minimum value; and (5) the 18 km level, generally obtained by interpolation, representative of the lower stratosphere, and found to play a role in LRT height variability [*Reid and Gage*, 1981]. At each of these levels we retain or compute pressure (p), geopotential height (Z), temperature (T), potential temperature (θ), and q_s. To compute q_s, we use the saturation vapor pressure formulation of *Dessler et al*. [1995]. We also retain p, Z, and T at the terminal level, usually the point of balloon burst, as well as some tropospheric temperature and lapse-rate data.

Individual soundings were eliminated from this analysis if any of the following conditions were met: (1) fewer than eight data levels were available; (2) data terminated below 10 km; (3) surface $T < -30°$C; (4) surface $p < 600$ hPa; (5) the LRT could not be identified, usually because the sounding did not extend at least 2 km above the would-be LRT; and (6) the observation was not within 3 hours of a standard synoptic observation time, 0000 or 1200 UTC.

2.2. Climatological Statistics

Monthly tropopause statistics were computed from individual soundings at each radiosonde site. Separate statistics for the 0000 and 1200 UTC observations were obtained whenever possible. For each variable, we computed the monthly mean and standard deviation, as well as the minimum, maximum, and quartile values. This paper focuses on the monthly mean data. Climatological monthly values were obtained by averaging values for each calendar month over the 30 year period of record 1961–1990. Monthly climatologies for a given station, calendar month, and time of observation were included if there were at least 3 months of data, each with at least 10 tropopause observations, during 1961–1990. This requirement eliminated 25 stations that had insufficient observations at both 0000 and 1200 UTC. The final network of 83 stations is shown in Figure 1a and listed in Table 1. On average, 18 years of data were available for each station, and more than 80% of the stations contributed data for at least 10 years.

As seen in Figure 2a, more soundings are available after about 1978 than before. A separate set of climatological means was obtained for 1978–1997, the most recent 20 year period for which we had data, to determine the sensitivity of the climatological values to a period of record.

Climatological values have been gridded at 10° latitude by 15° longitude resolution, with generally one or two stations per sampled grid box (Figure 1a). Grid box averages are means of the values at stations within the box. For presentation purposes, data void regions were assigned the zonal mean value based on the sampled boxes within the relevant latitude band.

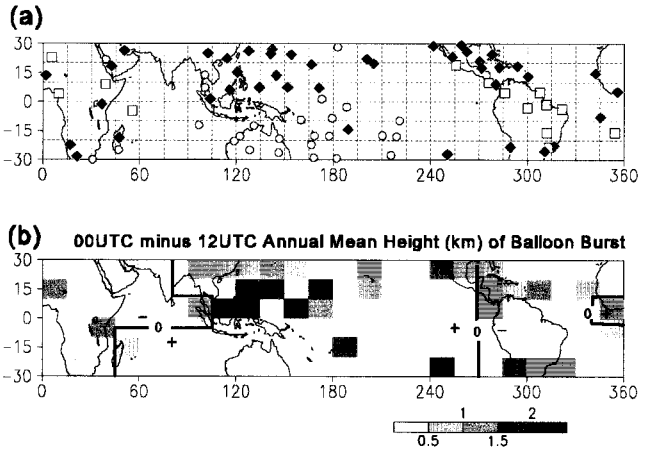

Figure 1. (a) Locations of radiosonde stations used in this study. Circles indicate only 0000 UTC data were used; squares indicate only 1200 UTC data were used; and diamonds indicate that data at both observation times were used. Gridding indicates the 10° latitude by 15° longitude grid used to develop climatological maps. (b) At locations having both 0000 and 1200 UTC data, shading shows the mean difference (0000 minus 1200 UTC) in the average height (km) of radiosonde sounding termination, generally due to balloon burst. Regions of positive and negative values are indicated by the plus and minus signs.

Separate climatological maps were created for 0000 and 1200 UTC, which were averaged to create maps for the combination of both observing times, with equal weighting for 0000 and 1200 UTC.

We present results for the tropical region 30°N–30°S and subregions thereof. For the purposes of this paper we define the equatorial zone as 10°N–10°S and the deep tropics as 15°N–15°S. The tropical regions poleward of 15° we refer to as the subtropics.

2.3. Sampling of the Tropical Tropopause

Although this 83 station network provides vastly better spatial coverage of the tropics than in earlier studies, serious data voids remain. As shown in Figure 1a, 54% of the grid is unsampled, with few stations in the eastern Pacific, the Indian Ocean, and Africa.

The typical level at which soundings terminate (generally due to balloon burst) is about 50 hPa or 21 km (Figure 2b), well above the tropical tropopause, whose nominal level is 100 hPa and 16 km. However, there are temporal and spatial variations that deserve mention.

The first issue relates to the day-night differences. At those stations consistently reporting twice daily, balloon burst statistics suggest that daytime soundings typically achieve higher heights than nighttime, with climatological differences of up to 2 km (Figure 1b). This is a well-known consequence of the fact that balloons are more frangible at lower nighttime temperatures. However, one disadvantage of daytime observations compared with nighttime is typically larger biases in the temperature data associated with solar radiation [*Luers and Eskridge*, 1998], which are particularly problematic early in the record [*Gaffen*, 1994]. As shown below (section 3.1), these effects lead to systematic differences between climatological 0000 and 1200 UTC data that may exceed or mask the true diurnal differences. Analysis of diurnal variations is necessarily

Table 1. Radiosonde Stations and Data Periods Used in This Paper

Name	Identification Number	Latitude	Longitude, °E	Elevation, m	Period	Observation Time, UTC
Abidjan, Ivory Coast	65578*	5.25	356.07	7	1961–1997	both
Addis Ababa, Ethiopia	63450	9.00	38.75	2362	1961–1997	1200
Antananarivo, Madagascar	67083	−18.80	47.48	1279	1967–1997	both
Antofagasta, Chile	85442	−23.42	289.53	114	1961–1997	both
Ascension Island	61902*	−7.97	345.60	86	1961–1997	both
Atuona, French Polynesia	91925*	−9.82	220.99	52	1968–1997	0000
Bahrain	40427	26.27	50.62	5	1961–1979	both
Bangkok, Thailand	48455*	13.73	100.55	16	1961–1997	both
Bauerfield, Vanuatu	91557	−17.70	168.30	20	1972–1997	0000
Belem, Brazil	82193	−1.38	311.52	16	1968–1997	1200
Belize, Belize	78583	17.53	271.70	5	1980–1997	both
Bloemfontein, South Africa	68424	−28.40	21.27	850	1976–1997	both
Bogota, Colombia	80222	4.70	285.85	2541	1965–1997	both
Brasilia, Brazil	83378	−15.86	312.07	1061	1966–1997	both
Broome, Australia	94203	−17.95	122.22	12	1965–1997	0000
Brownsville	72250	25.92	262.53	7	1961–1993	both
Canton Island, Kiribati	91701	−2.77	188.29	3	1961–1992	0000
Cayenne, French Guiana	81405	4.83	307.63	9	1964–1997	1200
Charleville, Australia	94510	−26.42	146.27	305	1961–1997	0000
Chi Chi Jima, Japan	47971	27.08	142.18	8	1967–1997	both
Clark Air Force Base, Philippines	98327	15.18	120.55	146	1961–1990	0000
Cocos Island	96996*	−12.18	96.83	5	1961–1997	0000
Curitiba, Brazil	83840	−25.51	310.83	908	1965–1997	both
Dahran, Saudi Arabia	40416	26.27	50.17	23	1978–1997	both
Dakar, Senegal	61641*	14.68	342.57	27	1961–1997	both
Darwin, Australia	94120*	−12.43	130.87	29	1961–1997	0000
Del Rio, Texas	72261	29.33	259.12	314	1961–1993	both
Douala, Cameroon	64910	4.02	9.70	10	1964–1997	both
Durban, South Africa	68588	−29.93	30.95	8	1961–1997	both
Easter Island	85469	−27.15	250.52	41	1966–1997	both
Fort-Dauphin, Madagascar	67197	−25.00	47.00	8	1972–1997	0000
Fortaleza, Brazil	82397	−3.72	321.45	19	1973–1993	1200
Funafuti, Tuvalu	91643*	−8.52	179.22	1	1973–1997	0000
Giles, Australia	94461	−25.03	128.30	580	1961–1997	0000
Guam	91217*	13.55	144.83	87	1961–1997	both
Hao, French Polynesia	91944	−18.10	219.10	3	1971–1997	0000
Hilo, Hawaii	91285	19.73	204.93	10	1961–1997	both
Honiara, Solomon Islands	91517*	−9.42	159.97	56	1961–1997	0000
Howard Air Force Base, Panama	78806	8.98	280.45	16	1961–1997	both
Isla Guadalupe, Mexico	76151	28.87	241.75	23	1971–1997	both
Iwo Jima, Japan	47981	24.78	141.33	106	1961–1990	both
Jeddah, Saudi Arabia	41024	21.67	39.15	10	1965–1997	both
Key West, Florida	72201	24.58	278.30	0	1961–1993	both
Khamis Mushait, Saudi Arabia	41114	18.30	42.80	2060	1978–1997	both
Kings Park, Hong Kong	45004	22.32	114.17	66	1961–1997	both
Kingston, Jamaica	78397	17.90	282.72	1	1961–1997	both
Koror, Palau	91408*	7.33	134.48	30	1961–1997	both
Kota Kinabalu, Malaysia	96471*	5.93	116.05	3	1969–1997	0000
Kunming, China	56778	25.02	102.43	1892	1961–1997	both
Lihue, Hawaii	91165	21.98	200.65	36	1961–1997	both
Majuro, Marshall Islands	91376*	7.10	171.40	3	1961–1997	both
Manaus, Brazil	82332	−3.15	300.02	84	1967–1997	1200
Manzanillo, Mexico	76654	19.07	255.67	3	1976–1997	1200
Mazatlan, Mexico	76458	23.18	253.58	4	1961–1997	both
Merida, Mexico	76644	20.97	270.48	9	1961–1997	both
Midway Island	91066	28.22	182.63	13	1961–1995	both
Minamitorishima, Japan	47991	24.30	153.97	9	1963–1997	both
Naha/Kagamizu, Japan	47936	26.23	127.68	80	1961–1997	both
Nairobi, Kenya	63741	−1.30	36.75	1798	1961–1997	both
Nandi, Fiji	91680	−17.75	177.43	16	1961–1997	0000
Niamey, Niger	61052*	13.48	2.17	233	1961–1997	both
Norfolk Island	94996	−29.05	167.93	110	1961–1997	0000
Noumea, New Caledonia	91592	−22.30	166.45	69	1961–1997	0000
Pago Pago, American Samoa	91765*	−14.33	189.28	3	1966–1997	both
Papeete, French Polynesia	91938	−17.55	210.39	2	1966–1997	0000
Port Hedland, Australia	94312	−20.38	118.62	6	1961–1997	0000
Raoul Island, New Zealand	93997	−29.25	182.08	36	1961–1997	0000
Rapa, French Polynesia	91958	−27.61	215.67	1	1966–1997	0000
Rio de Janeiro, Brazil	83746	−22.81	316.75	42	1961–1997	both
San Jose, Costa Rica	78762	10.00	275.80	920	1972–1997	1200

Table 1. (continued)

Name	Identification Number	Latitude	Longitude, °E	Elevation, m	Period	Observation Time, UTC
San Juan, Puerto Rico	78526	18.45	293.90	3	1961–1997	both
Sao Paulo, Brazil	83780	−23.62	313.35	802	1961–1997	both
Seawell, Barbados	78954*	13.07	300.50	47	1965–1997	both
Seychelles	63985*	−4.67	55.52	3	1976–1997	1200
Singapore	48698*	1.37	103.98	18	1961–1997	both
Songkhla, Thailand	48568*	7.18	100.62	4	1961–1997	both
St. Helena Island	61901	−15.97	354.30	436	1977–1997	1200
Tamanrasset, Algeria	60680	22.78	5.52	1378	1961–1997	both
Tarawa, Coral Sea Islands	91610	1.35	172.93	2	1961–1997	0000
Townsville, Australia	94294	−19.25	146.77	5	1961–1997	0000
Truk, Micronesia	91334*	7.47	151.85	3	1961–1997	both
Wake Island	91245	19.30	166.62	5	1961–1997	both
Windhoek, South Africa/Namibia	68110	−22.57	17.10	1715	1961–1985	both

Stations in the deep tropics used for the trend analysis of section 4.3 are indicated by an asterisk. The time of observation listed refers to the data incorporated in the climatology. Some stations for which both 0000 and 1200 UTC observations were included in the climatology had sufficient data for trend analysis at only one time.

limited by the fact that almost half of the stations in our network typically take only one observation daily (Table 1). At many stations, observations are made during daylight, so those stations nearer the Greenwich meridian generally report at 1200 UTC and those nearer the International Dateline generally report at 0000 UTC (Figure 1a).

A second issue involves the long-term variation in balloon burst statistics and the vertical resolution of the soundings. Figure 2b shows time series of the network-average pressure and height of sounding termination. There is general improvement (increasing heights, decreasing pressures) from 1960 to about 1990, with deterioration thereafter. In addition, the number of reported data levels (not shown) tends to increase over time, lending more confidence to the identification of the tropopause. Basing our climatological statistics on the period 1961–1990, we recognize the improvement of the soundings over this period, both with respect to the vertical resolution and coverage and with respect to data accuracy, which has generally improved with changes in instrumentation and observing practices. Later, we explore the impact of the averaging period on climatological statistics.

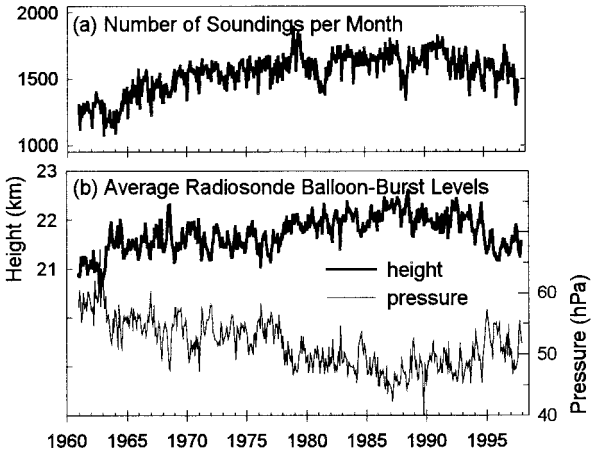

Figure 2. (a) Number of soundings per month used in this study, and (b) the average level of sounding termination, shown in terms of pressure and height.

3. Tropopause Characteristics

3.1. Tropopause Height

The tropical tropopause has a strong zonal structure. Therefore to summarize the characteristics of the LRT, CPT, and the 100 hPa level, Figure 3 presents climatological annual-mean zonal-mean values of tropopause Z, p, T, q_s, and θ. The values are plotted at the central latitude of each 10° latitude zone. Figure 4 presents comparable information on the longitudinal variability of these same variables in the equatorial zone. These two figures summarize the mean state of the tropopause, and we will return to them frequently.

As depicted in Figure 3a, the height of LRT, Z_{LRT}, shows considerable north-south variability, with values ranging from ~16.5 km in the deep tropics to less than 16 km in the southernmost latitude band in this analysis. The CPT is up to ~1 km higher than the LRT but exhibits very little variability with latitude (Figure 3a). The climatological annual-mean zonal-mean height of the tropical CPT is ~16.9 km. The CPT minus LRT height difference is smallest (~200–800 m) near the equator (Figure 3a), where the LRT is at its maximum height. The LRT and CPT definitions will indicate the same location if the coldest point of a sounding is at the base of an inversion layer deep enough (at least 2 km) to define the LRT. This situation is more likely in regions of frequent deep convection (the equatorial zone) than in regions of subsidence (the subtropics), where the cold point may reside at the top of a layer (whose base is the LRT) in which temperature is decreasing at a rate of 2 K/km or less. On annual average, the 100 hPa level is intermediate in height to the CPT and LRT, residing at ~16.6 km and, like the CPT, shows little north-south variability.

The proximity of the annual-mean climatological height of the 100 hPa level to the LRT and CPT, especially in the equatorial zone, is deceptive. Figure 5 shows the climatological mean seasonal cycles of the LRT, the CPT, and the 100 hPa level, in the equatorial zone (10°N–10°S), and the interannual variability about the monthly means. As shown in Figure 5a, the 100 hPa height is 16.5 km all year long, with minimal interannual variability, whereas the LRT and CPT are higher in NH winter (when the 100 hPa level is in the troposphere) and lower in NH summer (when the 100 hPa level is in the stratosphere). The seasonal cycles of CPT and LRT pressure

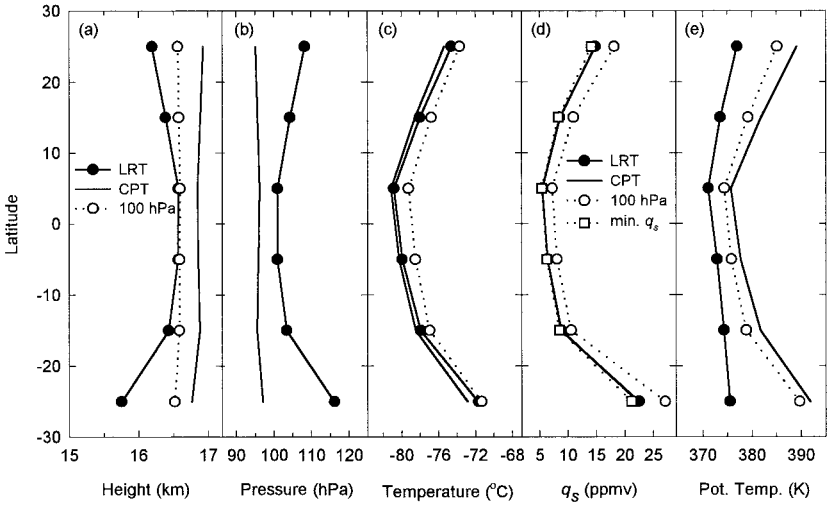

Figure 3. Climatological mean characteristics of the lapse-rate tropopause (LRT), cold-point tropopause (CPT), and 100 hPa level. Annual-mean zonal-mean (a) height, (b) pressure, (c) temperature, (d) water vapor saturation volume mixing ratio (q_s), and (e) potential temperature are based on gridded values computed from individual radiosoundings for 1961–1990 from the stations listed in Table 1. Data represent means for 10° latitude bands and are plotted at the midpoint of each band. In Figure 3d, annual-mean zonal-mean minimum values of $q_s(q_{s\min})$ are also shown.

(Figure 5b) support this interpretation. Because the CPT is the level of minimum temperature, the 100 hPa level, whether in the troposphere or stratosphere, is warmer (Figure 5c).

Further exploring the climatological seasonal variability of tropopause height, Figures 6a–6d show climatological monthly mean maps, based on data from both 0000 and 1200 UTC, of Z_{LRT} for four representative months: January, April, July, and October. Maps for intermediate months (not shown) indicate smooth transitions between the months depicted.

On annual average (shown in Figure 6e), Z_{LRT} is higher in the Northern Hemisphere (NH) than in the Southern Hemisphere (SH). This feature is more prominent in NH winter (December, January, February (DJF)), when Z_{LRT} maxima reach 17.1 km over the western Atlantic region, over the northern part of South America, and east of Central America. The location of the highest LRT is over north equatorial Africa during most of the rest of the year. Only in November is Z_{LRT} maximum over the tropical Pacific, near Wake Island. (We note the existence of three subtropical stations, Kunming, China; Dahran, Saudi Arabia; and Bahrain, which had very high Z_{LRT} values that we consider unrepresentative in comparison with other stations at comparable latitude.) The location of maximum Z_{CPT} (not shown) is somewhat similar, although not identical. It is over Central America, at ~17.6 km, in December through March, and over various parts of Africa during the remaining months. We note, in particular, that we do not find the highest CPT, LRT, or 100 hPa level over the western tropical Pacific warm pool region during any month of the year. Definitive statements about the spatial structure of the tropopause are not possible due to the poor coverage of the radiosonde network over the eastern Pacific, Indian, and Atlantic Oceans.

The January Z_{LRT} values shown in Figure 6a can be compared with DJF-average Z_{LRT}, based on 1991–1995 ECMWF analyses, shown by *Highwood and Hoskins* [1998, Figure 4b]. This depiction shows Z_{LRT} between 16.25 and 16.75 km over almost the entire domain of the current analysis, except over Indonesia, where they show lower values. This contrasts with

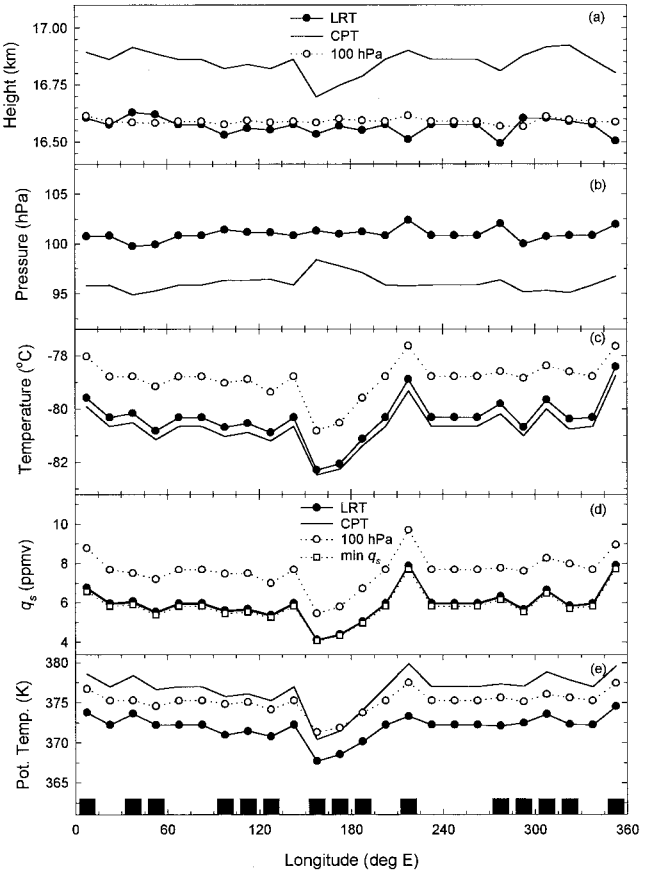

Figure 4. Climatological annual-mean (a) height, (b) pressure, (c) temperature, (d) water vapor saturation volume mixing ratio, and (e) potential temperature in the equatorial zone (10°N–10°S) at the LRT, CPT, and 100 hPa level. In Figure 4d, $q_{s\min}$ data are also shown. Data points represent regions of 15° longitude width; those sampled by the radiosonde network are indicated by the squares along the abscissa in Figure 4e. Unsampled regions have been assigned the zonal-mean values for presentation purposes.

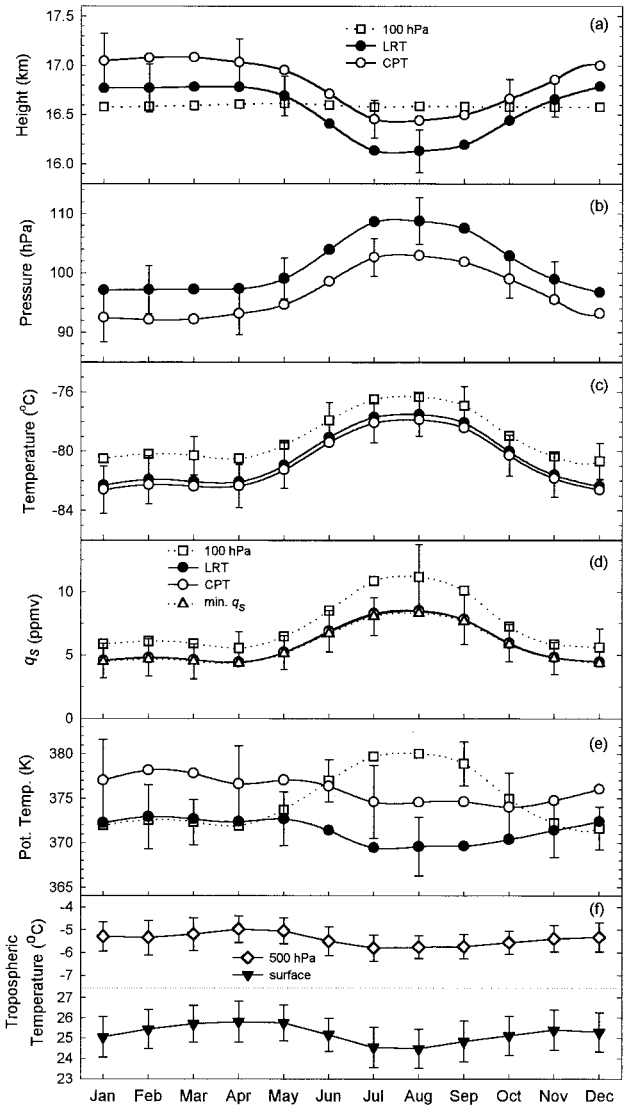

Figure 5. Climatological seasonal cycles of (a) height, (b) pressure, (c) temperature, (d) water vapor saturation volume mixing ratio, and (e) potential temperature in the equatorial zone (10°N–10°S) at the LRT, CPT, and 100 hPa level. Tropospheric temperatures at the surface and 500 hPa level in the same region are shown in Figure 5f. Error bars indicate ±1 interannual standard deviations about the 1961–1990 monthly means. Except in Figures 5d and 5f, error bars are shown every third month, alternating among the three levels, to avoid clutter. In Figure 5d, error bars are shown every fourth month. In Figure 5a the error bars for the 100 hPa level fall within the square symbols.

our depiction of higher values, by at least 0.5 km, throughout the tropics, and more complex spatial structure, which is only partly explained by our use of more closely spaced contour intervals. The lack of structure in the work of *Highwood and Hoskins* [1998] is not due to the 3 month averaging period; we find the same inconsistency in comparison with DJF averages from our data set. It is probably the result of the poorer vertical resolution of the ECMWF model in comparison with the radiosonde observations. Maps of Z_{LRT} presented by *Hoinka* [1999], based on ECMWF reanalysis data, show a similar low bias compared both with the radiosonde data shown here and with the climatological fields presented by *Makhover* [1979].

How precise are the estimated climatological mean values shown in Figure 6? The standard error of the monthly climatological means can be expressed as $\varepsilon/n^{1/2}$, where ε is the typical random measurement error in geopotential height of a significant level (such as the tropopause) in radiosonde data, and n is the number of samples. (Here we use ε in lieu of the more commonly used σ, which we employ differently below.) Given $\varepsilon \approx 72$ m [*WMO*, 1996], and $n \approx 600$ (the typical number of soundings from any station used in computing the climatological mean), the standard error associated with the monthly climatological means is approximately 3 m.

As an estimate of the interannual variability of Z_{LRT}, Figure 6e shows the climatological annual means, and Figure 6f shows the interannual standard deviations σ. The σ values were computed from the station data (with their variable periods of record (Table 1)), and the gridded values are computed in the same manner as the gridded monthly averages. Typical interannual σ values are a few hundred meters, with somewhat lower values closer to the equator. Thus the systematic differences, (>0.5 km) between Figure 6a and *Highwood and Hoskins* [1998] far exceed the uncertainty in the radiosonde data due to measurement error, but they seem to be within $\pm 2\sigma$ of the radiosonde-based interannual variability.

A source of smaller variations in tropopause height results from a different synoptic time of observations. Figure 7 shows 0000 minus 1200 UTC annual- and meridional-average differences in Z_{LRT}, Z_{CPT}, and Z_{100}, based on data from stations making regular observations at both observation times. These average differences are generally less than 50 m for the LRT and 100 hPa level and less than 100 m for the CPT. However, there is a somewhat systematic bias, with daytime Z generally exceeding nighttime values. Three possible explanations for this pattern are (1) the tropopause is higher during the day because the underlying troposphere is warmer; (2) daytime deep convection pushes the tropopause to higher levels than at night; (3) radiosonde temperature data have characteristically different errors in day and night, due to the effects of solar radiation impinging on the temperature sensors. The first two factors are true diurnal variations in tropopause height, while the third is an artificial signal, and it seems likely that each contributes to the pattern in Figure 7.

While Figure 3 allows direct comparison of the climatological annual-mean zonal-mean characteristics of the LRT, CPT, and 100 hPa levels, Figure 8 presents a more thorough comparison of the heights of these levels, including three estimates of the variability about the means shown in Figure 3a. For each level, Figure 8 shows the 1961–1990 climatological annual-mean zonal-mean Z (solid circles and solid line), duplicating the depiction of Figure 3a. To depict the meridional (within zone) variability about the zonal-mean values, we show (using dashed lines) the maximum and minimum climatological annual-mean values within each 10° latitude band. The seasonal (within year) variability is similarly represented (using dotted lines) by maximum and minimum climatological zonal-mean monthly values. The interannual variability is represented as ± one standard deviation of the yearly annual-mean zonal-mean values about the climatological annual mean zonal mean and is shown using open circle symbols connected by a solid line. To illustrate the effect of the averaging period on the climatological means, we present annual-mean zonal-mean values based

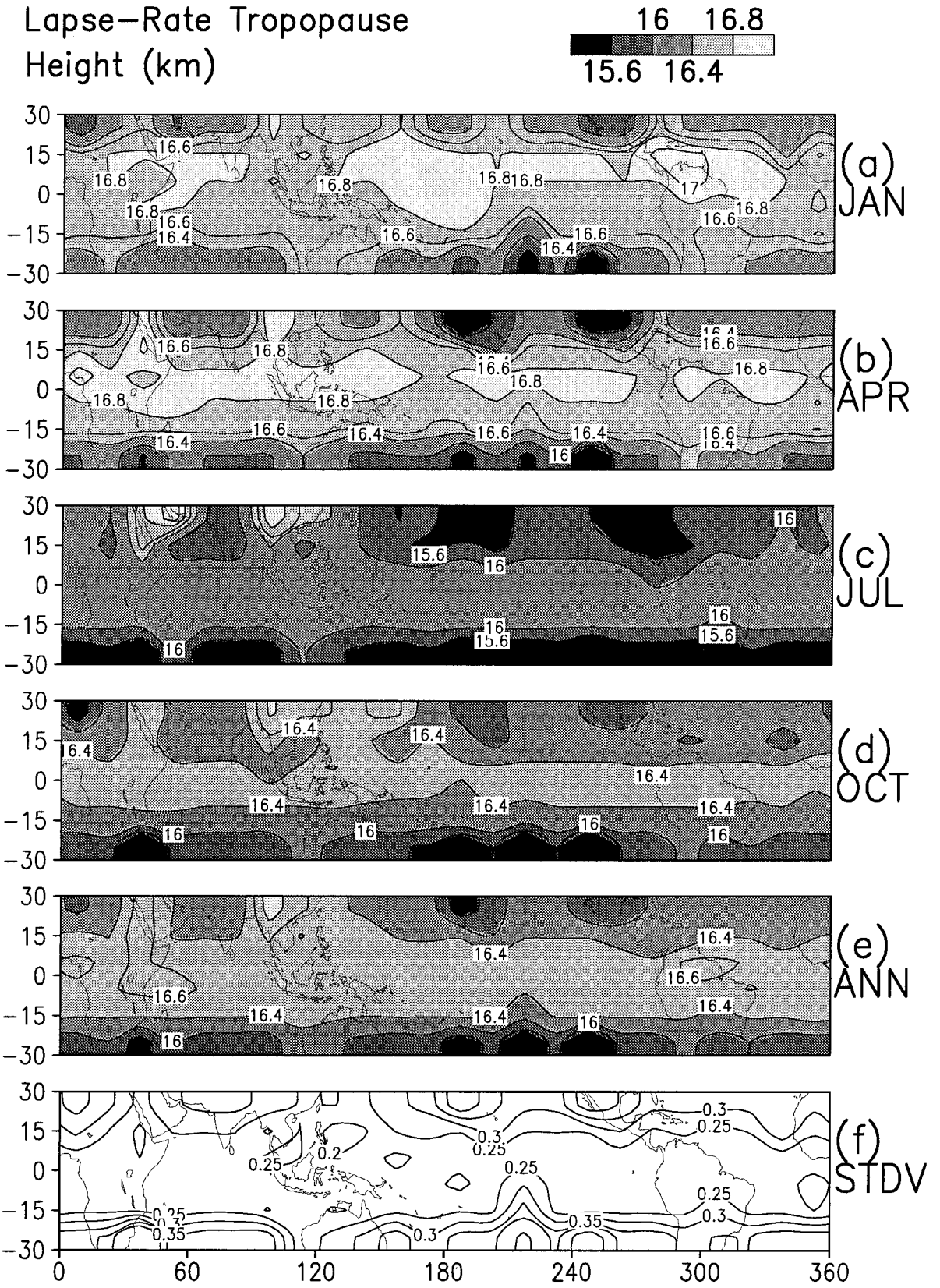

Figure 6. Climatological mean height (km) of the lapse-rate tropopause based on 0000 and 1200 UTC data for 1961–1990. Data based on radiosonde station values have been gridded, and unsampled grid boxes were assigned the zonal-mean value for presentation purposes. Contours are every 0.4 km; additional contours are shown at 16.6 and 17.0 km. Monthly means for (a) January, (b) April, (c) July, and (d) October are shown, as are (d) annual means and (e) the interannual standard deviation of the individual annual means about the long-term annual means.

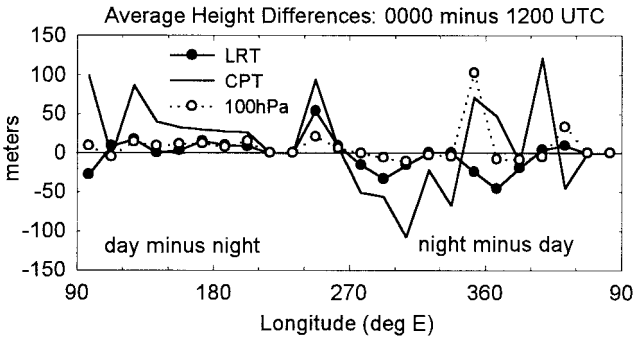

Figure 7. Difference in annual-average height, between 0000 and 1200 UTC, of the lapse-rate tropopause, the cold-point tropopause, and the 100 hPa level, as a function of longitude. Values at each longitude represent averages among all stations between 30°N and 30°S in a 15° longitude interval.

on 1978–1997 data (solid triangles and solid line) for comparison with the 1961–1990 values.

The LRT (Figure 8a) and CPT (Figure 8b) exhibit significantly more variability than the 100 hPa level (Figure 8c). The seasonal, longitudinal, and interannual variation in LRT and CPT height are about 0.5–1.5 km, while the 100 hPa level varies by about 0.1 km. This significantly lower variability of Z_{100}, combined with its lack of correspondence to Z_{LRT} and Z_{CPT} in terms of seasonal structure (Figure 5a), shows that Z_{100} is, in general, a poor substitute for tropopause height. The differences between the 1961–1990 and the 1979–1997 means are much smaller than the zonal, seasonal, or interannual variability. This suggests very little sensitivity of tropopause height statistics to the data period, although the slightly higher values for 1979–1997 suggest a possible increase in tropopause height over time.

3.2. Tropopause Pressure

The structure of the tropical tropopause seen in climatological p fields is generally consistent with that shown in the Z fields. The pressure of the CPT is about 96 hPa, in an annual-mean zonal-mean sense, while the LRT is found between 100 and 115 hPa (Figure 3b). The differences between p_{CPT} and p_{LRT} are a few hectopascals in the equatorial zone (Figure 4b) and more than 10 hPa in the subtropics (Figure 3b). The maximum annual-mean equatorial p_{CPT} values are just west of the International Dateline (Figure 4b). The monthly locations of minimum p_{CPT} and p_{LRT} are over Central America in NH winter (when $p_{\mathrm{LRT}} \approx 91$ hPa and $p_{\mathrm{CPT}} \approx 83$ hPa) and over Africa during other months, fully consistent with the locations of maximum Z_{CPT} and Z_{LRT}, respectively, discussed in the preceding subsection.

Similarly, the seasonal variations in tropopause p are consistent with seasonal variations in Z, as seen by comparison of Figures 5a and 5b and Figures 6 and 9. Figure 9 demonstrates that p_{LRT} has strong zonal symmetry, is lower in NH winter than in summer, and has seasonal and interannual variations of comparable magnitude. This latter feature can also be seen in Figure 10, which summarizes the variability of tropopause pressure about the climatological annual-mean zonal-mean values.

The annual and interannual variations in p_{LRT} and p_{CPT} values are ~10 to 15 hPa (Figures 10a, 10b), and they exceed the meridional variability, particularly in the equatorial zone (see Figure 4b). This result confirms that the 20–30 hPa vertical resolution of reanalysis products is insufficient for detailed depictions of the spatial and seasonal variations of the tropical tropopause. Diurnal differences in tropopause p (not shown) are consistent with those for Z (Figure 7), with lower pressure in daytime than at night. As with Z, tropopause p values for 1978–1997 are close to 1961–1990 values, with a slight indication of lower p_{CPT} values in the more recent period (Figure 10b).

3.3. Tropopause Temperature

Figure 3c shows climatological annual-mean zonal-mean tropopause T values, which are lowest in the NH equatorial zone. The CPT is only slightly colder than the LRT, which is colder than the 100 hPa level. The higher 100 hPa level temperatures are the result of the fact that the 100 hPa level is generally in the upper troposphere during NH winter and in the lower stratosphere in NH summer, and both regions are warmer than the tropopause. The difference between T_{LRT} and T_{CPT} is generally <1 K in the tropics as a whole and <0.5 K in the equatorial zone. The differences in Z, p, and T at the LRT and CPT outside the equatorial zone depicted in Figures 3a–3c suggest the frequent existence of a second LRT (coinciding with the CPT) above the first LRT. Indeed, we find that second tropopauses are 3–4 times as frequent poleward of 10° latitude than in the deep tropics.

The zonal structure of annual-mean tropopause T in the equatorial zone, shown in Figure 4c, shows a distinct minimum (<-82°C) in the 150°–165°E region (above Honiara and Truk) and slightly higher values in the region 165°–180°E (above Funafuti, Noumea, Tarawa, and Wake Island). Surprisingly, comparison of Figures 4a, 4b, and 4c shows that within the equatorial zone, on annual average, the longitudes at which the tropopause is coldest are not also those at which it is at highest height and lowest pressure. On the contrary, the CPT is coldest in the 150°–165°E region, where it is at the lowest height and the highest pressure.

How significant is this feature? The difference in T_{LRT} between the region of minimum T_{LRT} (in the western tropical Pacific) and the region of minimum p_{LRT} and maximum Z_{LRT} (in the western tropical Atlantic) is ~3 K, which is not large compared with local interannual σ values of 1–2 K (Figure 11f), which suggests that the minimum T region is not fixed from year to year. It is also possible that the difference may be related to observational uncertainty. The 0000–1200 UTC difference in T is typically 0.2–1.4 K. Thus about half of the temperature difference between the regions of highest and lowest tropopause heights may be explained by interannual and diurnal variability.

On the other hand, the temperature difference is not simply an artifact of temporal averaging but reveals itself on monthly and daily timescales. In the equatorial zone the tropopause is coldest, and at lowest pressure and highest height, during NH winter, as shown in Figures 5a, 5b, and 5c. Comparison of the January climatological mean maps of Z_{LRT} (Figure 6a), p_{LRT} (Figure 9a), and T_{LRT} (Figure 11a) reveals different locations of the extreme values in January. On the monthly timescale in the equatorial zone we find that the location of minimum monthly mean T_{LRT} corresponds to the location of minimum monthly mean p_{LRT} (or maximum Z_{LRT}) during only 18% (or 19%) of the months during 1961–1990. Comparable percentages are even lower for the CPT, whose minimum T location corresponds to the minimum $p(Z)$ location during only 9%

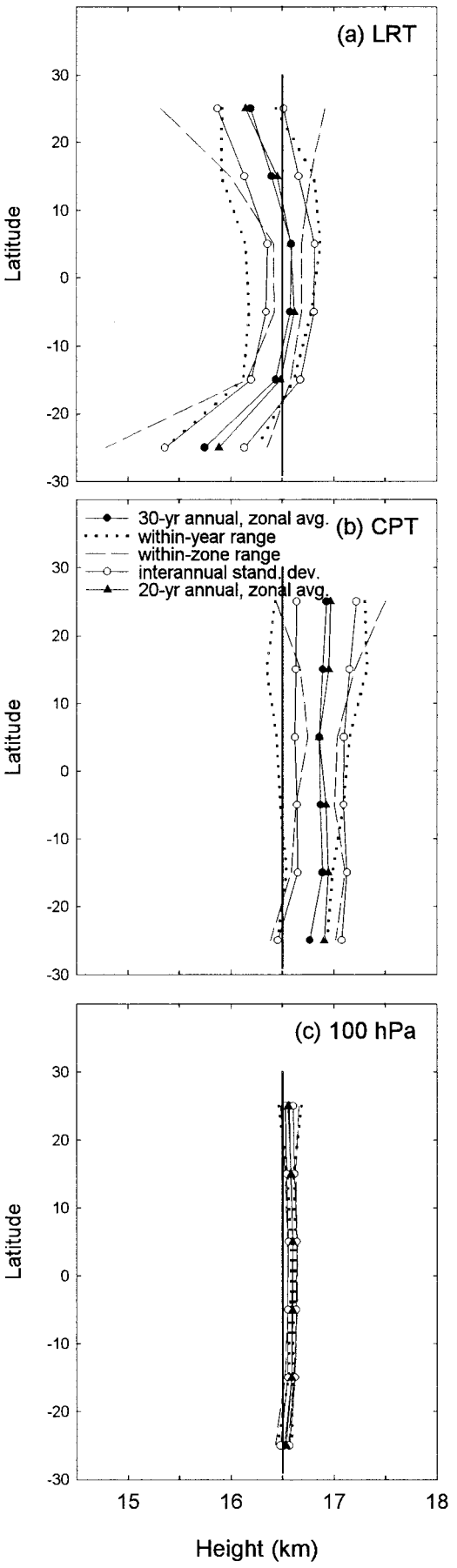

(7%) of the months. We obtain very similar results with daily data. Thus, in general, we do not find the tropopause to be coldest where it is highest or at lowest pressure.

The seasonal variability of equatorial tropopause T (Figure 5c) contrasts with that of tropospheric T (Figure 5f). The former is dominated by the annual harmonic, while the latter (both at the surface and at 500 hPa) has a semiannual signal, with maxima following the equinoxes. Some indication of this semiannual harmonic appears in Z_{LRT} and Z_{CPT} (Figure 5a), which we expect to vary with the temperature of the underlying troposphere. A closer examination of the two 10° latitude bands, which constitute the equatorial zone (i.e., equator to 10°N and equator to 10°S), reveals that zonal-average T_{LRT} and T_{CPT} are lower in the NH band than in the SH band in all months. This is in contrast with tropopause Z (and p), which varies seasonally and is higher (and lower, respectively) in the winter hemisphere.

The seasonal variations in tropopause T indicate that lowest climatological monthly mean temperatures (−85°C) are observed in NH winter in this region east of Indonesia (Figure 11). In NH summer and early fall the tropopause is coldest (−81°C) in the region farther west, over Singapore, Thailand, and Malaysia; during April and November it is coldest (−84°C) over Bogota. As the tropopause Z field, these features of the T field are in reasonably good agreement with the January and July climatological analyses of *Makhover* [1979], although the latter study found three regions of January minimum T_{LRT}, two of which are south of the equator. However, both Figure 11 and *Makhover* [1979] show lower tropopause temperatures than shown by *Hoinka* [1999]. Our finding of minimum tropopause temperature in NH winter over the western Pacific region is consistent with earlier studies based on less comprehensive radiosonde data sets [*Newell and Gould-Stewart*, 1981; *Highwood and Hoskins*, 1998], although as mentioned above, we do not find minimum tropopause pressure in this region, as did *Highwood and Hoskins* [1998], or maximum tropopause heights.

Figure 12 compares the seasonal, meridional, and interannual variability in T_{LRT}, T_{CPT}, and T_{100}. For each level, the three sources of variability are of comparable magnitude (a few degrees Celsius), although the meridional variability is smaller in the deep tropics than in the subtropics. Comparison of the 1961–1990 and the 1978–1997 CPT and LRT T data suggests a slight cooling of the tropopause over time (Figure 12). We explore this issue further in section 4.3.

Figure 8. (opposite) Climatological zonal-mean annual-mean heights for the period 1961–1990 (solid circles and solid line) and for the period 1978–1997 (triangles and solid line) of (a) the lapse-rate tropopause, (b) the cold-point tropopause, and (c) the 100 hPa level. Data represent means for 10° latitude bands and are plotted at the midpoints. The maximum and minimum climatological monthly and zonal averages are shown by the dotted lines, as a measure of seasonal (within year) range. The maximum and minimum climatological annual average values at different longitudes within a latitude band are shown by the dashed lines, as a measure of longitudinal (within zone) range. The 1961–1990 interannual variability, represented by ±1 standard deviation of the individual-year annual-mean zonal means about the 30 year average annual-mean zonal mean, is shown by the open circles and solid line. For ease of comparison, a reference line is plotted at 16,500 m in each panel.

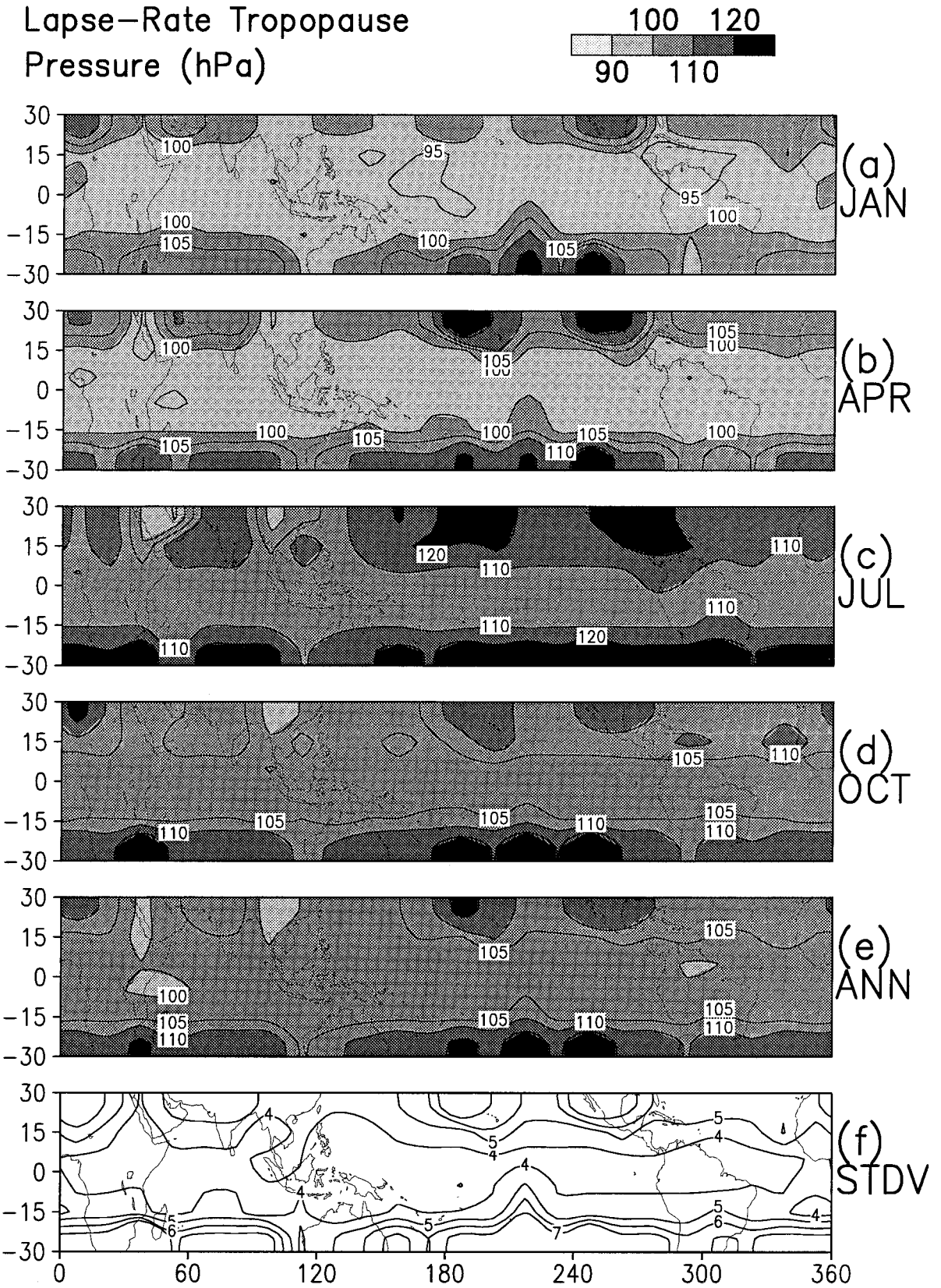

Figure 9. As in Figure 6 but for pressure (hPa). Contours are every 10 hPa; additional contours are shown at 95 and 105 hPa.

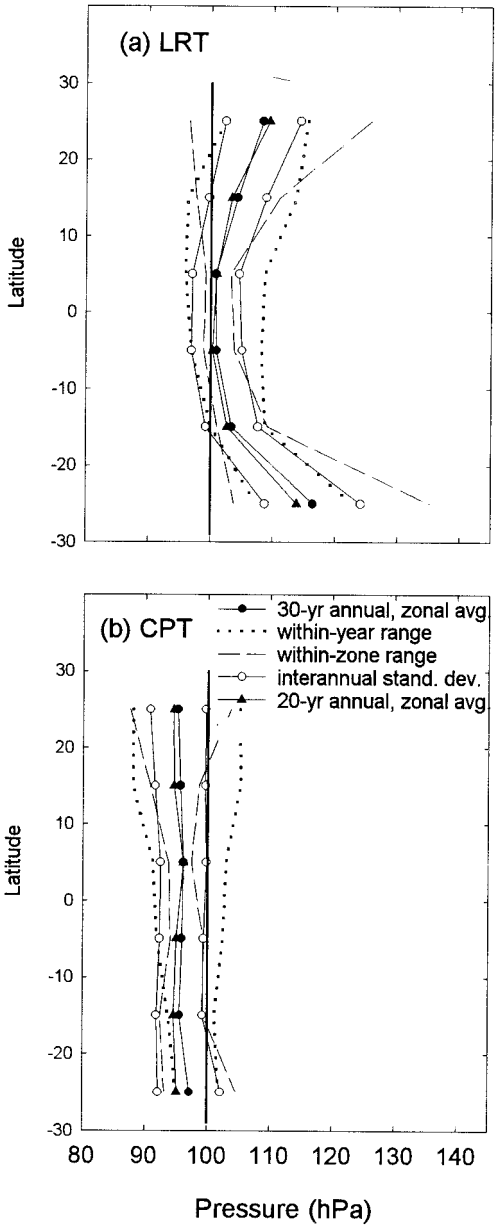

Figure 10. As in Figure 8 but for pressure at the (a) lapse-rate tropopause and (b) cold-point tropopause. The reference lines are at 100 hPa.

3.4. Tropopause Saturation Mixing Ratio of Water Vapor

Stratospheric water vapor is thought to have two main sources: (1) oxidation of stratospheric methane and (2) transport of water vapor from the troposphere to the stratosphere. In the tropical lower stratosphere, the second source is considered dominant, and flux through the tropical tropopause, as opposed to higher latitudes, is the major source, due to the poleward direction of stratospheric flow [*Mote et al*., 1996; *Dessler*, 1998]. As hypothesized by *Newell and Gould-Stewart* [1981], cross-tropopause water vapor flux may be limited to the coldest regions of the tropical tropopause, where T and therefore q_s values are low enough to explain the very low stratospheric q observations. This "stratospheric fountain" mechanism, which calls for preferential regions of cross-tropopause transport (notably the deep convective regions above the western Pacific/Indian Ocean warm pool), has been called into question by *Dessler* [1998], whose analysis of recent observed stratospheric q data and q_s from radiosonde observations suggests that transport need not be limited spatially. *Vömel and Oltmans* [1999] suggest, and *Zhou et al*. [2000] present evidence, that recent q_s values may be lower than a few decades ago, so the need to invoke preferred regions may have been more important a few decades ago than now.

Newell and Gould-Stewart [1981] based their argument on q_s computed from monthly mean 100 hPa data, and *Dessler* [1998] based his on minimum q_s evaluated from individual soundings. (*Dessler* [1998] used minimum q_s ($q_{s\min}$) rather than CPT q_s because of the small pressure influence on q_s calculations.) Here we present q_s computed at the LRT, CPT, and 100 hPa level, as well as $q_{s\min}$.

The seasonal variations in $q_{s\min}$, shown in Figure 13 (and in Figure 5d for the equatorial zone), indicate drier conditions in the NH winter than in summer. Local climatological monthly mean $q_{s\min}$ values occur at approximately the same locations as the T_{CPT} minima discussed in section 4.3, although there are some minor differences. The lowest values (2.4–2.9 ppmv) are in the region 0°–10°N and 135°–175°E (over Koror, Majuro, Tarawa, and Truk) during December, January, and February. During other months the local minima, ranging from 3.1 to 5.5 ppmv, can be found within the region 90°–180°E. On annual average (Figures 13e and 4d), much of the equatorial belt has climatological $q_{s\min}$ values of 5.8 ± 2.6 ppmv (where 2.6 is approximately twice the interannual σ value (Figure 13f)).

Comparison of the annual-mean $q_{s\min}$ values shown in Figure 13e with annual-mean q values at the tropopause from the ECMWF reanalysis [*Hoinka*, 1999, Figure 5a] reveals important differences. *Hoinka* [1999] shows values ranging from 5.0 to 7.5 ppmv over most of this domain, except for lower values (2.5–5.0 ppmv) over the western tropical Pacific between 15°N and 15°S. Our $q_{s\min}$ values (which are saturation values, whereas the values in the work of *Hoinka* [1999] are meant to be actual values) are larger than shown by *Hoinka* [1999] poleward of about 15° latitude. However, in the deep tropics our $q_{s\min}$ values are generally lower, which is consistent with our lower T_{LRT} values. Figure 13e also shows a much stronger latitudinal gradient in mixing ratio than *Hoinka* [1999], which is not evident in the T_{LRT} maps. Because of the uncertainties in the model depictions of humidity at the tropopause level, it is unclear whether the smooth fields presented by *Hoinka* [1999] are realistic.

Figure 14 shows the climatological annual-mean zonal-mean $q_{s\min}$, as well as the variability about the means. Comparable plots for the LRT and CPT (not shown) are visually indistinguishable because q_s values at the LRT and CPT are generally not more than 5% greater than $q_{s\min}$. Thus although CPT and LRT pressures (and heights) can be significantly different, the closeness of their temperatures (Figures 3c, 4c, 5c) means that climatological q_s determinations are nearly identical at both tropopause locations (Figures 3d, 4d, 5d). At 100 hPa, q_s is 10–25% higher than $q_{s\min}$ because of the higher temperatures at 100 hPa.

Climatological zonal-average, annual-average values of $q_{s\min}$ are 5–6 ppmv in the equatorial zone (Figure 14), but over the western Pacific, where the tropopause is coldest, values are about 4 to 5 ppmv (Figure 4d). The 100 hPa q_s data shown in Figure 4d demonstrates that use of 100 hPa T to assess tropopause q_s results in an overestimate of ~2 ppmv.

The estimates of zonal, seasonal, and interannual variability

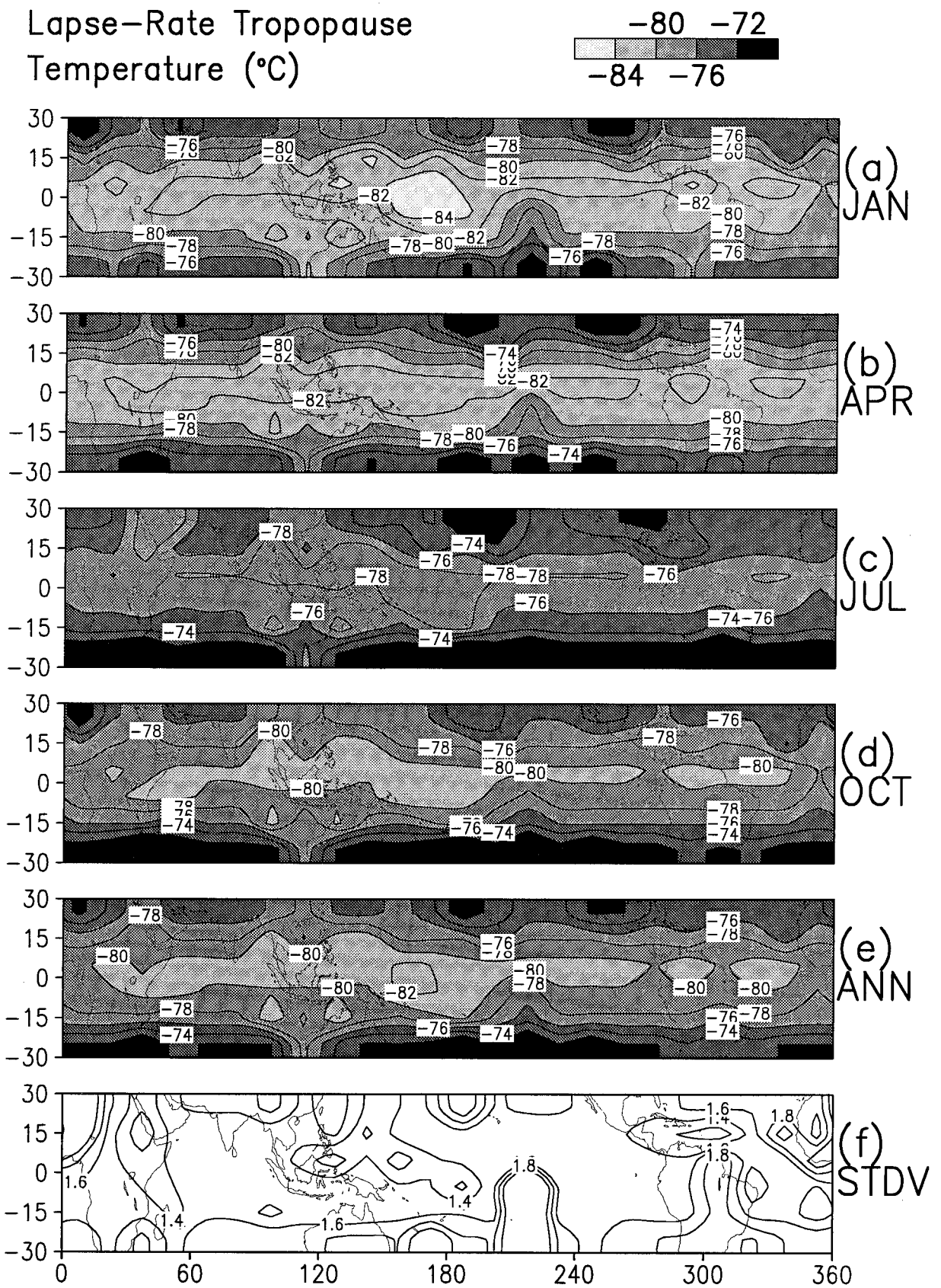

Figure 11. As in Figure 6 but for temperature (°C). Contours are every 2°C.

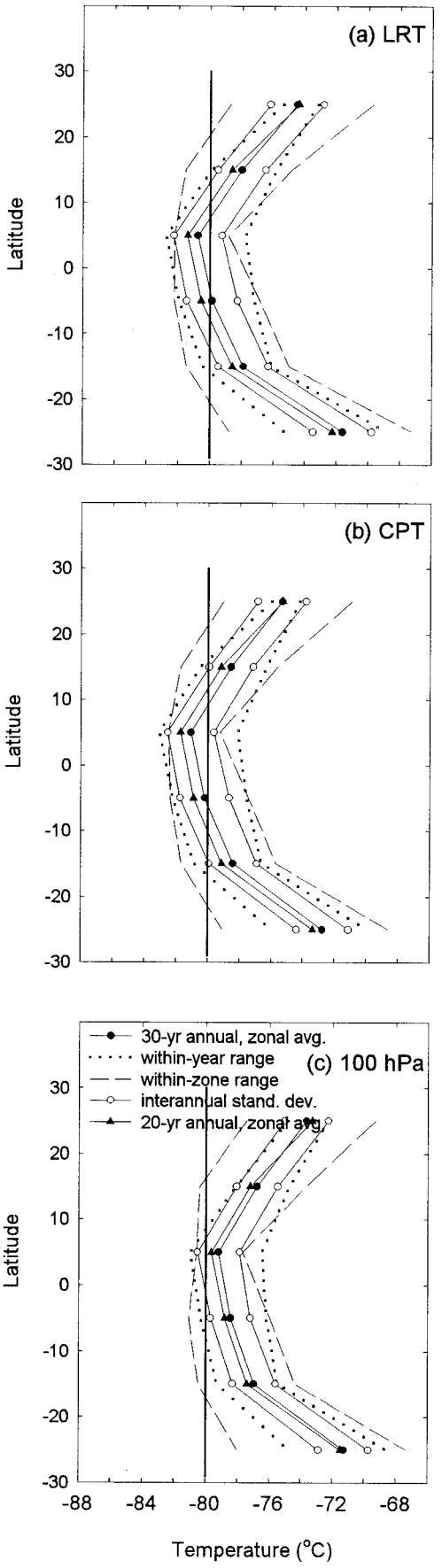

Figure 12. As in Figure 8 but for temperature. Reference lines are at −80°C.

in $q_{s\min}$ values are comparable in magnitude to the annual-mean zonal-mean $q_{s\min}$ values themselves (Figure 14). Further contributing to the temporal variability of $q_{s\min}$ are the diurnal variations, as estimated by the 0000 minus 1200 UTC means (not shown). These range from 0.1 to 0.5 ppmv in the deep tropics to 1.7 ppmv in the subtropics, so this measure of diurnal variability can be as large as 10% of the mean.

Climatological values of $q_{s\min}$ for 1961–1990 are larger than for 1978–1997 (Figure 14); the average value for the equatorial zone is 5.1 ppmv for the later period, compared with 5.8 ppmv for the earlier period. This difference is partly due to artificially high values in the early 1960s due to radiation effects on the radiosondes, as discussed above. The more reliable 1978–1997 estimate is higher than the 4.0 ± 0.8 ppmv estimated by *Dessler* [1998] of the equatorial average value of each sounding's $q_{s\min}$ based on data for 1994–1997. However, the annual average values given by *Dessler* [1998] are based on weighting the NH winter data twice as much as the NH summer data, to account for the seasonal cycle in mass transport through the tropopause. Because NH winter values are about one third lower than summer values (Figure 5d), we expect, and find, our unweighted average values to be higher than the *Dessler* [1998] values. For the 1994–1997 period we obtain average equatorial q_s of 4.1 ppmv. These results suggest a decrease in $q_{s\min}$ during recent decades, as discussed below (section 4.3), and are qualitatively consistent with *Zhou et al.* [2000b].

3.5. Tropopause Potential Temperature

Potential temperature, which is defined as $\theta = T(1000/p)^{\kappa}$, is lower (~375 K) at the LRT than at the 100 hPa level, which has lower values than the CPT (Figure 3e), as would be expected from the p and T values at each level (Figures 3b and 3c). There is a general increase in θ from the equator to 30° latitude, which is more marked for the 100 hPa level and the CPT than for the LRT.

The seasonal variation of θ_{LRT}, shown in Figure 15, reaches its peak in the equatorial zone during NH spring (see also Figure 5e), in agreement with the study of the Truk radiosonde record by *Reid and Gage* [1996]. Since θ is a function of both T and p, the high spring values are a consequence of the fact that T_{LRT} has started to increase from its NH winter minimum (Figure 11), but p_{LRT} remains close to its winter level (Figure 9). The upwelling driven by extratropical wave forcing in the lower stratosphere [*Holton et al.*, 1995] reaches its peak in NH winter and spring [*Rosenlof et al.*, 1995] and would be expected to cool the tropopause region. The accompanying rise in height, and drop in pressure, of the tropopause is less easily explained, but *Reid and Gage* [1996] have suggested that it might be caused by deeper penetration of convection resulting from cooling of the uppermost troposphere and a consequent decrease in the local stability. These two tendencies have opposite effects on θ_{LRT}. Nevertheless, the seasonal variation in θ is quite marked, possibly because the expected decrease in T_{LRT} is at least partially offset by radiative warming. The larger seasonality in the NH compared with the SH is also probably a result of the strong enhancement of wave forcing during NH winter and spring.

As shown in Figure 5e, the seasonal variations of θ_{100} are larger than and out of phase with the seasonal variations of θ_{LRT} and θ_{CPT}. This further reinforces the notion of the 100 hPa level as a poor indicator of the tropical tropopause. It is also worth noting that θ_{LRT} rarely reaches 380 K (Figure 16), the value suggested by *Holton et al.* [1995] as relevant to strato-

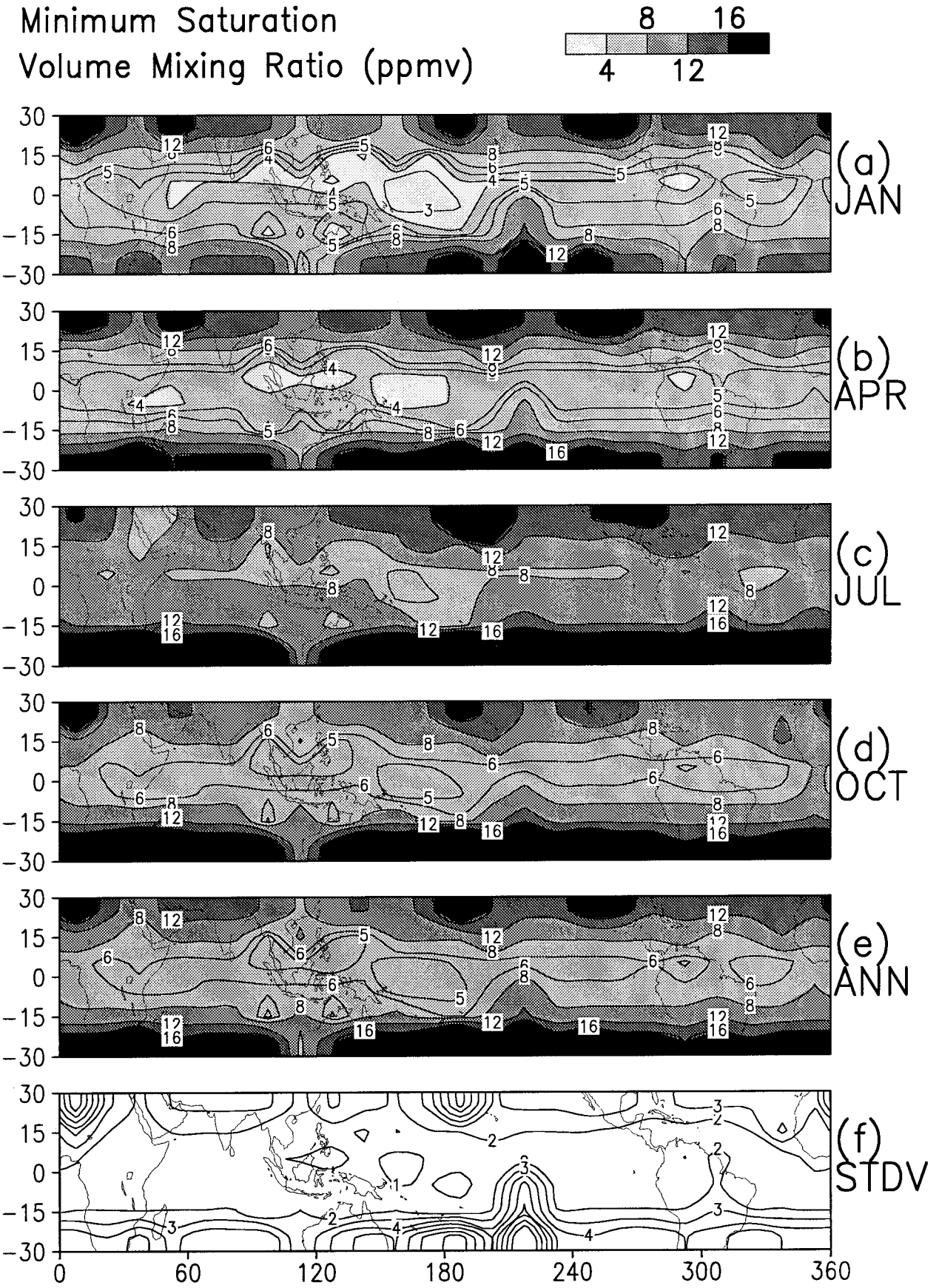

Figure 13. As in Figure 6 but for minimum water vapor saturation volume mixing ratio (ppmv). Contours are every 4 ppmv; additional contours are shown at 3 and 5 ppmv.

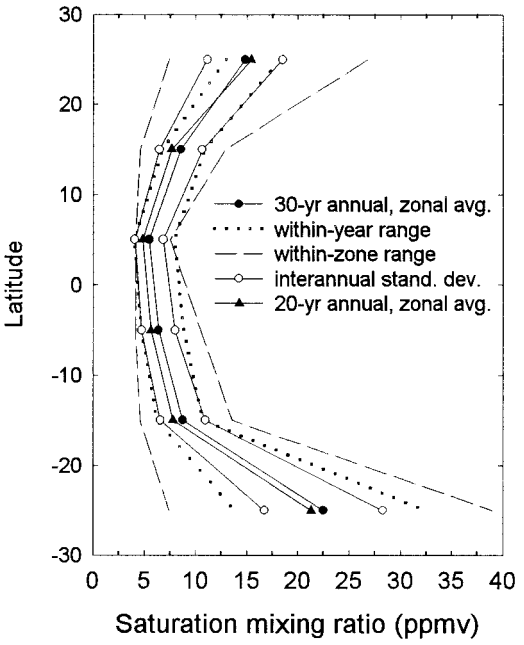

Figure 14. As in Figure 8 but for minimum water vapor saturation volume mixing ratio.

sphere-troposphere exchange in the tropics. Values of θ in the equatorial zone are typically between 365 and 375 K at the LRT and between 370 and 380 K at the CPT (Figures 5e and 16).

4. Interannual Variability of the Tropopause in the Equatorial Zone

In the previous sections we compared climatological mean features of the LRT, CPT, and 100 hPa level, including seasonal and spatial variations and the magnitude of interannual standard deviations. In this section we further explore the nature of interannual variations in the tropical tropopause. Because of the strong zonal nature of the tropopause, and to focus attention on the potential role of the tropical tropopause as a source of stratospheric water vapor, the analysis focuses on the interannual variability of spatial means, in the equatorial zone, 10°N–10°S (in sections 4.1 and 4.2) and in the deep tropics, 15°N–15°S (in section 4.3).

4.1. Correlations Among Tropopause Characteristics

For the period 1978–1997, we created time series of spatial-mean monthly anomalies of tropopause characteristics, based on 0000 and 1200 UTC data from 18 stations in the equatorial zone. Linear correlation coefficients, r, computed after detrending these time series, are shown in Table 2.

Pressure and height anomalies at the CPT and at the LRT are highly anticorrelated. In addition, Z_{LRT} is anticorrelated with p_{CPT}, and vice versa. These negative correlations are an expected result of hydrostatic balance. Saturation mixing ratio anomalies are highly correlated with temperature anomalies and moderately well correlated with pressure anomalies, consistent with the Clausius-Clapeyron relationship.

Temperature and height anomalies at the CPT and LRT are anticorrelated. In contrast, at the 100 hPa level, T and Z are weakly positively correlated. This result is consistent with the notion that the 100 hPa level in the equatorial zone is often below the LRT and CPT (within the troposphere) during much of the year (Figure 5a), so positive height anomalies are associated with positive tropospheric T anomalies. Correlations between anomalies of T_{LRT} and other variables are approximately the same as correlations involving T_{CPT} anomalies. The same holds for Z.

Interannual potential temperature anomalies are essentially uncorrelated with T anomalies at the LRT and CPT. However, θ is inversely correlated with p and positively correlated with Z, consistent with findings of *Gage and Reid* [1987], using data for 1971–1981 from five stations in the tropical Pacific. This is in contrast with the obvious positive spatial correlation of longitudinal variations of annual mean T and θ (Figures 4c and 4e) and of January values (Figures 11a and 15a).

These correlations basically confirm our understanding of atmospheric structure and thermodynamics and underscore some of the findings of previous sections regarding the differences and similarities among the LRT, CPT, and 100 hPa levels. They are a useful guide for studies with other data sets that may not offer so wide an array of tropopause characteristics for analysis.

4.2. Correlations With the Stratosphere and Troposphere

Having established a high degree of association among various tropopause parameters, we now explore interannual variability in the tropical tropopause as it may relate to changes in both the troposphere and the lower stratosphere. Using the same region and time period as in the previous section, Table 3 presents correlations between monthly anomalies of T_{LRT} and Z_{LRT} and several other variables. Correlations based on the CPT are not shown here because they are almost identical to those based on the LRT. Similarly, we do not show correlations with LRT p, θ, or q_s, which can be deduced, at least qualitatively, from the correlations with T and Z.

There is little correlation between T_{LRT} and any of the surface or tropospheric variables examined, which include surface pressure p_s and temperature T_s; 500 hPa height Z_{500} and temperature T_{500}; the lapse rate in the surface-300 hPa layer $\gamma_{\mathrm{sfc\text{-}300}}$; and the virtual temperature of the 850–100 hPa layer $T_{850\text{-}100}$. The height of the LRT, on the other hand, is positively correlated ($r \approx 0.5$) with each of these, except p_s ($r = 0.04$) and $\gamma_{\mathrm{sfc\text{-}300}}$ ($r = -0.41$). Thus the height of the tropical tropopause reflects the temperature of the underlying troposphere and decreases with decreasing atmospheric stability, suggesting an indirect response to convection. The positive correlation between the Z_{LRT} and T_s and the negative correlation with the tropospheric lapse rate are both consistent with the theoretical results of *Thuburn and Craig* [1997, 2000], based on radiative model calculations. The positive interannual correlations between Z_{LRT} and $T_{850\text{-}100}$ is consistent with the model of the tropical tropopause developed by *Reid and Gage* [1981], and with the findings of *Reid and Gage* [1996], who noted that the seasonal cycle of Z_{LRT} is in phase with that of 700–125 hPa thickness (which is proportional to virtual temperature).

The lack of correlation between T_{LRT} and either surface or tropospheric temperature is evident in Figure 17a, which shows tropical-mean anomaly time series based on data from 20 stations in the deep tropics. (The time series for the 18 station equatorial network used in the correlation analysis are very similar. The larger spatial domain will be discussed in the next section, but the time series aid in understanding the correlation results here.) Note the much larger amplitude fluctuations in

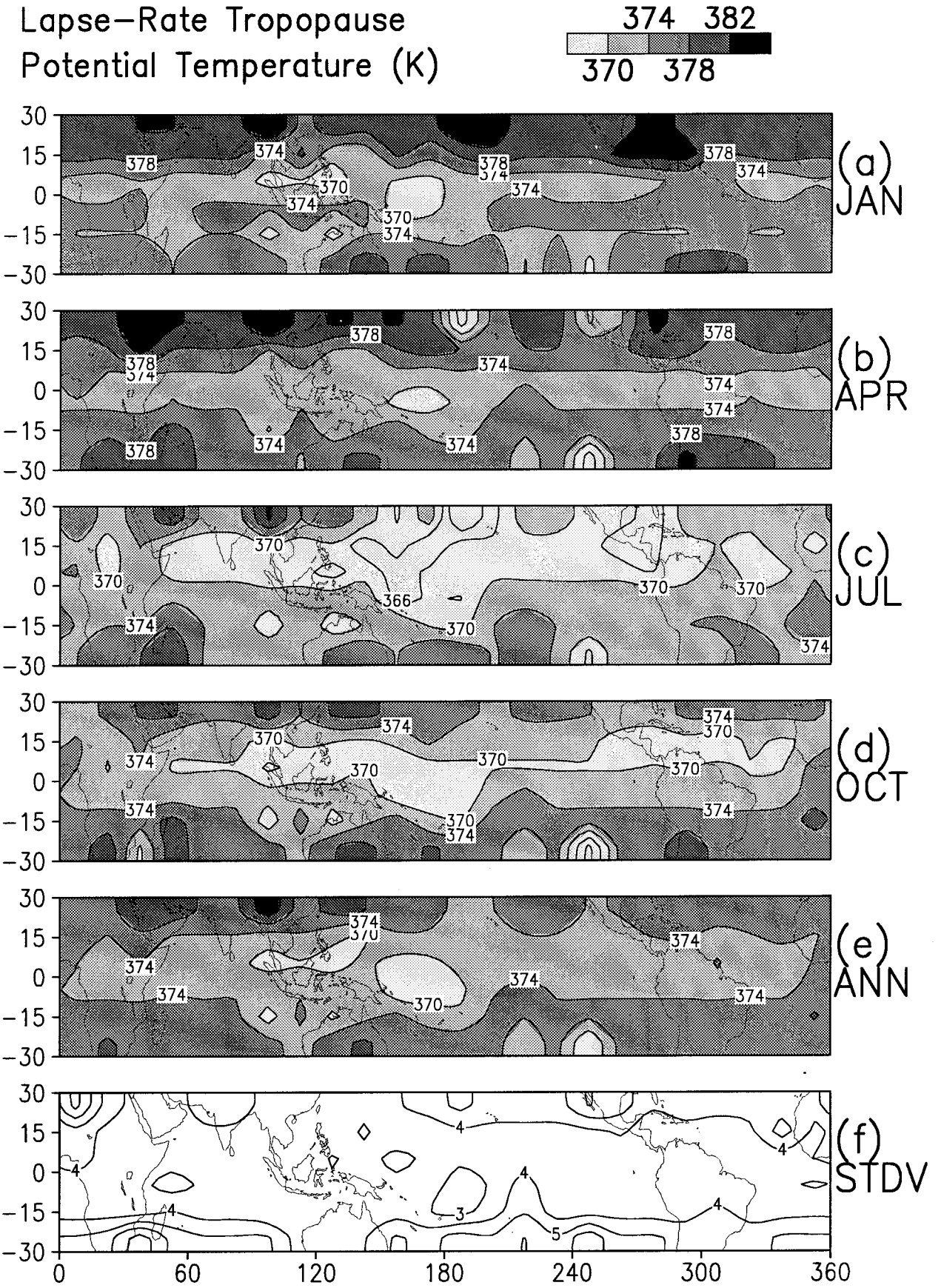

Figure 15. As in Figure 6 but for potential temperature (K). Contours are every 4 K.

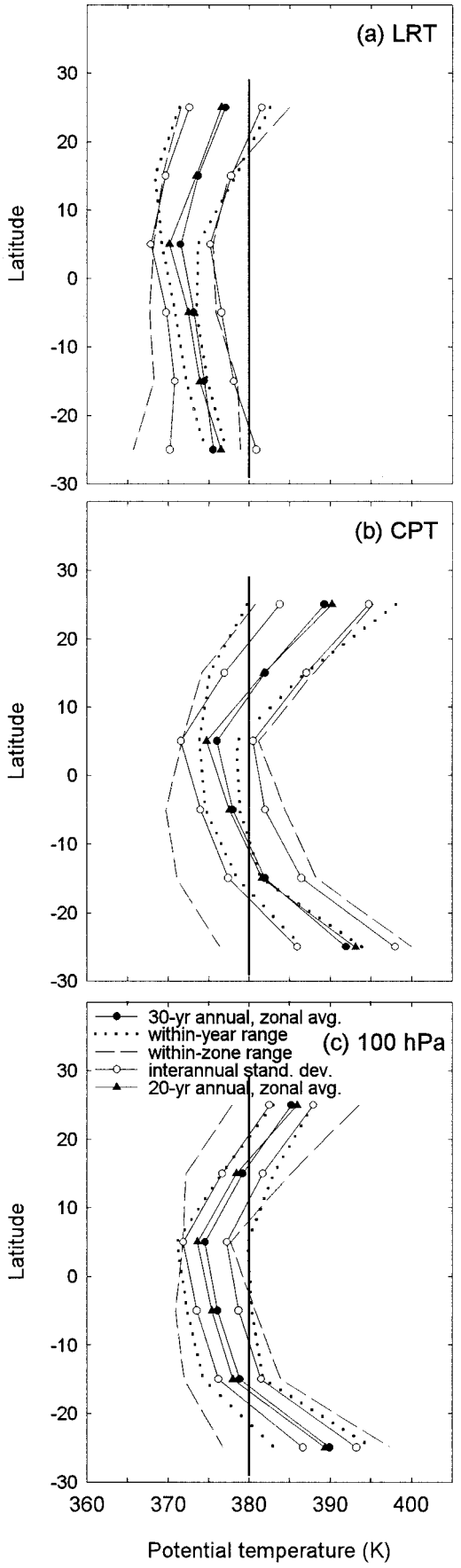

Figure 16. As in Figure 8 but for potential temperature. Reference lines are at 380 K.

T_{LRT} than in $T_{850\text{-}100}$ or T_s. The latter are dominated by the El Niño-Southern Oscillation signal (for example, the warmings in 1982–1983 and 1986–1987). On the other hand, T_{LRT} has some of the character of the 18 km T anomalies, including a quasi-biennial oscillation (QBO), as noted by *Angell and Korshover* [1974], and warming following the 1982 El Chichón volcanic eruption, although there is little evidence of warming after the 1991 eruption of Mount Pinatubo.

Indeed, we find T_{LRT} to be correlated with stratospheric (18 km) temperature T_{18} and pressure p_{18}, as shown in Table 3. The height of the LRT is negatively correlated with T_{18}, and the magnitude of the correlation ($r = -0.80$) exceeds the correlation of Z_{LRT} with any tropospheric parameters, suggesting a greater stratospheric than tropospheric influence. Thus tropopause temperature seems to vary with the lower stratosphere, while tropopause height varies with both the lower stratosphere and the troposphere, including the surface. These findings call into question the chain of reasoning employed by *Kirk-Davidoff et al*. [1999], who suggest a potential depletion of stratospheric ozone in the Arctic in association with an increase in tropical surface temperatures, via a sequence of linked changes, one of which is an increase in tropical tropopause temperature with increasing T_s. We find no such relationship on an interannual basis, nor, as discussed in the next section, on a 20 year timescale. In addition, as discussed in section 3.3, the seasonal variability of surface and tropopause temperature are poorly correlated (Figures 5a and 5f).

We note, however, that this correlation analysis has addressed only equatorial-average interannual variations. More extensive analysis, to isolate different timescales of variability and to examine local correlations and teleconnections, could reveal additional features.

4.3. Long-Term Tropopause Changes

To assess possible long-term trends in the tropical tropopause, we examined records from 20 stations in the deep tropics, shown in Figure 18 and noted in Table 1. Stations were included in the analysis if data were available for at least 85% of the months for the period 1978–1997. Figure 17 shows time series of mean temperature anomalies at 18 km, the LRT, the 850-100 hPa layer, and the surface, as well as Z_{LRT} and $q_{s\min}$. Visual examination of the temperature time series suggests cooling at 18 km and at the LRT, little change in the troposphere, and warming at the surface. The surface and tropospheric temperature trends are discussed in more detail by *Gaffen et al*. [2000a] and are shown here primarily to contrast with the long-term behavior of the tropopause temperature.

Station values of T_{LRT} temperature trends are shown in Figure 18. Note that three stations have two trend values plotted, the upper one is based on 0000 UTC data and the lower on 1200 UTC data. In only one case is the trend positive, in one case it is zero, and all of the remaining 21 trend estimates are negative, ranging from -0.03 to -0.18 K decade^{-1}. However, these trends may be influenced by changes in instruments and methods of radiosonde observation, which have been shown to affect long-term temperature records [*Gaffen et al*., 2000b]. For example, Figure 19 shows T_{LRT} anomaly time series for three stations: Koror, Truk, and Majuro. For several decades, observations at these stations were made using VIZ brand radiosondes. In December 1995 the observatories at Koror and Truk switched to Vaisala radiosondes, which is associated with abrupt decreases in T_{LRT} of 3 to 4 K at these two stations

Table 2. Correlations Among Monthly Anomaly Time Series of Tropopause Characteristics Based on Data for 1978–1997 From Stations in the Equatorial Zone 10°N–10°S

	Z_{LRT}	p_{LRT}	T_{LRT}	θ_{LRT}	$q_{s\mathrm{LRT}}$	p_{CPT}	Z_{CPT}	T_{CPT}	θ_{CPT}	$q_{s\mathrm{CPT}}$	Z_{100}	T_{100}	θ_{100}	q_{s100}	$q_{s\mathrm{min}}$
Z_{LRT}	(1.00)	(−0.99)	(−0.69)	(0.84)	(−0.55)	(−0.92)	(0.93)	(−0.69)	(0.62)	(−0.58)	(0.51)	(−0.53)	(−0.53)	(−0.55)	(−0.58)
p_{LRT}	(−0.99)	(1.00)	(0.78)	(−0.77)	(0.67)	(0.92)	(−0.89)	(0.77)	(−0.53)	(−0.68)	−0.36	(0.64)	(0.64)	(0.65)	(0.67)
T_{LRT}	(−0.69)	(0.78)	(1.00)	−0.19	(0.92)	(0.64)	(−0.55)	(1.00)	0.01	(0.93)	0.15	(0.92)	(0.92)	(0.83)	(0.93)
θ_{LRT}	(0.84)	(−0.77)	−0.19	(1.00)	−0.08	(−0.79)	(0.85)	−0.20	(0.86)	−0.09	(0.72)	−0.03	0.03	−0.14	−0.09
$q_{s\mathrm{LRT}}$	(−0.55)	(0.67)	(0.92)	−0.08	(1.00)	(0.51)	(−0.41)	(0.91)	0.12	(0.99)	0.23	(0.92)	(0.92)	(0.92)	(0.99)
p_{CPT}	(−0.92)	(0.92)	(0.64)	(−0.79)	(0.51)	(1.00)	(−0.99)	(0.67)	(−0.75)	(0.52)	−0.39	(0.48)	(0.48)	(0.49)	(0.53)
Z_{CPT}	(0.93)	(−0.89)	(−0.55)	(0.85)	(−0.41)	(−0.99)	(1.00)	(−0.58)	(0.82)	(−0.42)	(0.54)	(−0.36)	(−0.36)	(−0.39)	(−0.43)
T_{CPT}	(−0.69)	(0.77)	(1.00)	−0.20	(0.91)	(0.67)	(−0.58)	(1.00)	−0.02	(0.92)	(0.15)	(0.91)	(0.91)	(0.82)	(0.93)
θ_{CPT}	(0.62)	(−0.53)	0.01	(0.86)	0.12	(−0.75)	(0.82)	−0.02	(1.00)	0.13	(0.65)	0.18	0.18	0.09	0.12
$q_{s\mathrm{CPT}}$	(−0.58)	(0.68)	(0.93)	−0.09	(0.99)	(0.52)	(−0.42)	(0.92)	0.13	(1.00)	0.22	(0.92)	(0.92)	(0.93)	(1.00)
Z_{100}	(0.51)	−0.36	0.15	(0.72)	0.23	−0.39	(0.54)	0.15	(0.65)	0.22	(1.00)	0.28	0.28	0.19	0.22
T_{100}	(−0.53)	(0.64)	(0.92)	−0.03	(0.92)	(0.48)	(−0.36)	(0.91)	0.18	(0.92)	0.28	(1.00)	(1.00)	(0.93)	(0.93)
θ_{100}	(−0.53)	(0.64)	(0.92)	0.03	(0.92)	(0.48)	(−0.36)	(0.91)	0.18	(0.92)	0.28	(1.00)	(1.00)	(0.93)	(0.93)
q_{s100}	(−0.55)	(0.65)	(0.83)	−0.14	(0.92)	(0.49)	(−0.39)	(0.82)	0.09	(0.93)	0.19	(0.93)	(0.93)	(1.00)	(0.93)
$q_{s\mathrm{min}}$	(−0.58)	(0.67)	(0.93)	−0.09	(0.99)	(0.53)	(−0.43)	(0.93)	0.12	(1.00)	0.22	(0.93)	(0.93)	(0.93)	(1.00)

Values shown in parentheses are significantly different from zero at the 95% confidence level, taking into account the lag-1 autocorrelation of the time series.

relative to Majuro, where VIZ radiosondes continued to be used (Figure 18). Thus it seems likely that the calculated cooling at Koror and Truk is overestimated because of this data artifact. *Zhou et al*. [2000b] adjust the radiosonde data for such instrument changes by fitting the time series to an equation with terms representing annual and semiannual harmonics, the QBO, sea surface temperature variations, linear trend, and an intervention term timed to coincide with known instrument changes. Because such adjustments can profoundly alter trend estimates [*Gaffen et al*., 2000], we make no such attempt here.

Instead, to determine the impact of such changes on T_{LRT} trends, we identified two subgroups of stations in the network. One group of three stations (Bangkok, Majuro, and Seawell), shown with boxes around the trend values in Figure 18, used the same type of instrument (VIZ radiosondes) during the entire 20 year period. A second group included these three stations plus four more (Cocos Island, Darwin, Guam, and Pago Pago, shown with circles in Figure 18) for which we could identify no obvious shifts in the time series that corresponded to instrument changes.

Figure 20 shows trends in Z, p, T, and θ at the LRT, and $q_{s\mathrm{min}}$, based on each of these three networks. Although the magnitude of the trends differ in each network (partly due to the effects of data inhomogeneities and partly due to the different spatial sampling), the sign of the trend is generally unaffected. These data show an increase in Z_{LRT} of about 20 m decade^{-1}, a decrease in p_{LRT} of about 0.5 hPa decade^{-1}, a cooling of about 0.5 K decade^{-1}, little change in θ_{LRT}, and a decrease in $q_{s\mathrm{min}}$ of about 0.3 ppmv decade^{-1}.

Using a subset of stations from the data set presented here, *Randel et al*. [2000] obtain a comparable T_{LRT} trend of −0.57 K decade^{-1} during 1979–1997. That trend reduces to −0.28 K decade^{-1} when the 1982–1983 data are omitted, to avoid the impact of the El Chichón eruption, which highlights the sensitivity of trends to anomalies near the ends of short data records [*Randel et al*., 2000]. Using radiosonde data for 1973–1998 and accounting for possible effects of radiosonde instrument changes, as well as sea surface temperature variations and the QBO, *Zhou et al*. [2000] report a trend in the temperature at the level of $q_{s\mathrm{min}}$ of −0.57 K decade^{-1}. *Simmons et al*. [1999] report a 100 hPa T trend of −0.6 K decade^{-1} based on the reanalysis and operational analyses from ECMWF for 1979–1998. Although the 100 hPa level is not representative of the tropopause, as discussed above, these similar trends are not surprising given the high correlation between T_{LRT} and T_{100} (Table 2). Indeed, the T_{LRT} time series in Figure 17 shares the main features of the T_{100} time series shown by *Pawson and Fiorino* [1998] for 1979–1995 from the ECMWF and NCEP reanalyses.

In interpreting these linear trend estimates we should bear in mind the highly nonlinear behavior of the time series in Figure 17. In particular, the decrease in $q_{s\mathrm{min}}$ is dominated by

Table 3. Correlations Among Monthly Anomaly Time Series of Tropopause Characteristics and Tropospheric and Stratospheric Variables, Based on Data for 1978–1997 From Stations in the Equatorial Zone (10°N–10°S)

	T_{LRT}	Z_{LRT}	p_s	T_s	Z_{500}	T_{500}	$T_{850\text{-}100}$	$\gamma_{\mathrm{sfc\text{-}300}}$	p_{18}	T_{18}
T_{LRT}	(1.00)	(−0.69)	0.02	−0.12	0.06	0.00	0.13	−0.06	(0.45)	(0.74)
Z_{LRT}	(−0.69)	(1.00)	0.04	(0.50)	(0.50)	(0.56)	(0.49)	(−0.41)	0.20	(−0.80)
p_s	0.02	0.04	(1.00)	0.13	0.17	0.00	0.02	−0.04	0.09	0.04
T_s	−0.12	(0.50)	0.13	(1.00)	(0.55)	(0.63)	(0.67)	−0.25	(0.53)	(−0.36)
Z_{500}	0.06	(0.50)	0.17	(0.55)	(1.00)	(0.79)	(0.77)	(−0.65)	(0.76)	−0.29
T_{500}	0.00	(0.56)	0.00	(0.63)	(0.79)	(1.00)	(0.91)	(−0.77)	(0.81)	−0.29
$T_{850\text{-}100}$	0.13	(0.49)	0.02	(0.67)	(0.77)	(0.91)	(1.00)	(−0.76)	(0.87)	−0.22
$\gamma_{\mathrm{sfc\text{-}300}}$	−0.06	(−0.41)	−0.04	−0.25	(−0.65)	(−0.77)	(−0.76)	(1.00)	(−0.71)	0.18
p_{18}	(0.45)	0.20	0.09	(0.53)	(0.76)	(0.81)	(0.87)	(−0.71)	(1.00)	0.10
T_{18}	(0.74)	(−0.80)	0.04	(−0.36)	−0.29	−0.29	0.22	0.18	0.10	(1.00)

Values shown in parentheses are significantly different from zero at the 95% confidence level, taking into account the lag-1 autocorrelation of the time series.

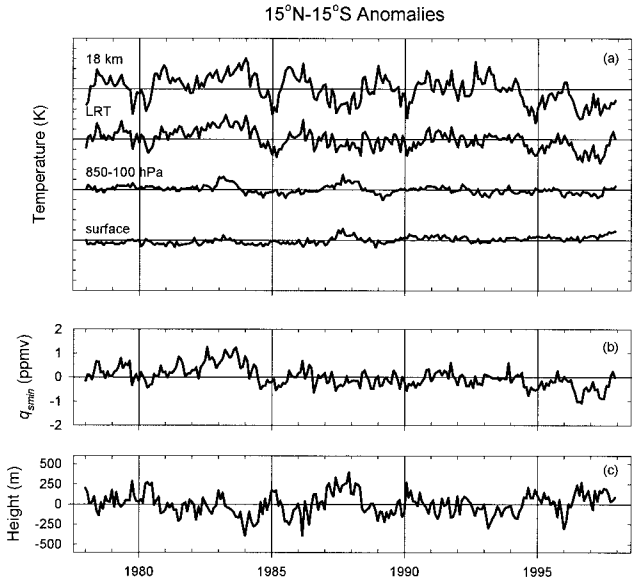

Figure 17. Time series of monthly anomalies, in the deep tropics (15°N–15°S), of (a) temperature at 18 km, temperature of the lapse-rate tropopause, virtual temperature in the 850-100 hPa layer, and surface temperature; (b) minimum water vapor saturation volume mixing ratio; and (c) height of the lapse-rate tropopause. In Figure 17a, each tick mark on the temperature scale represents 1 K.

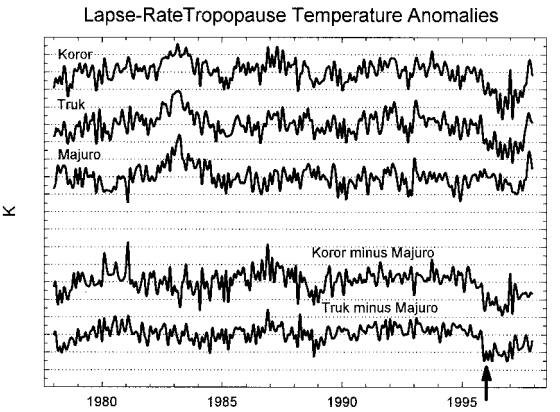

Figure 19. Lapse-rate tropopause monthly temperature anomalies at three stations: Koror, Truk, and Majuro. Also shown are differences, Koror minus Majuro, and Truk minus Majuro. The arrow indicates date (December 1995) of the change from VIZ to Vaisala radiosonde types at Koror and Truk. Tick marks on the vertical scale are at 1 K intervals; dotted grid lines are at 2 K intervals.

the large positive anomalies during the early 1980s and the large negative anomalies in the late 1990s. This decrease is in contrast to the observed (relatively smooth) increase in stratospheric water vapor over Boulder, Colorado, during 1981–1994 measured by balloon-borne frost-point hygrometers [*Oltmans and Hofmann*, 1995]. However, the $q_{s\min}$ change is much smaller during the 1990s, when measurements from the Halogen Occultation Experiment also show increasing stratospheric water vapor concentrations [*Nedoluha et al.*, 1998; *Evans et al.*, 1998], and there is a suggestion of increasing $q_{s\min}$ in the early 1990s. The LRT cooling we find for 1978–1997 is in contrast to the warming found by *Angell and Korshover* [1974] for the period 1960–1970.

5. Summary

This paper has presented a temporally and spatially comprehensive depiction of the tropical tropopause, based on radiosonde data from 83 stations covering the period 1961–1997. Figures 3, 4, and 5 summarize various characteristics of the lapse-rate tropopause (LRT), cold-point tropopause (CPT), and the 100 hPa level. Our major findings are as follows:

1. The climatological (1961–1990) annual-mean zonal-mean LRT height varies from ~16.5 km in the equatorial zone to less than 16 km in the subtropics. The CPT resides at ~16.9 km, with very little north-south variability. The annual-mean zonal-mean pressure of the LRT is close to 100 hPa in the equatorial region but higher in the subtropics. The CPT is generally at lower pressure, with an annual-mean zonal-mean location of about 96 hPa. The CPT is slightly colder than the LRT. In the equatorial zone the annual-mean zonal-mean CPT temperature is about −81°C, with corresponding water vapor saturation volume mixing ratio of 4 to 6 ppmv, depending on the data period.

2. The tropopause is higher, colder, at lower pressure, and

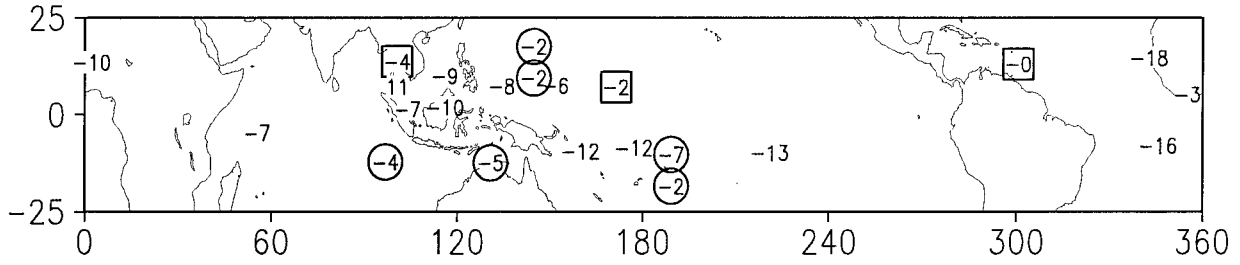

Figure 18. Temperature trends for 1978–1997 at the lapse-rate tropopause, in 0.01 K decade^{-1}. At three stations (Guam, Kota Kinabalu, and Pago Pago), two values are given; the top value is for 0000 UTC and the bottom one is for 1200 UTC. Station values that are circled represent stations whose time series show no obvious evidence of artificial shifts in mean value that may be due to changes in instruments or observing methods. Station values surrounded by squares indicate that only VIZ radiosondes were used during this period.

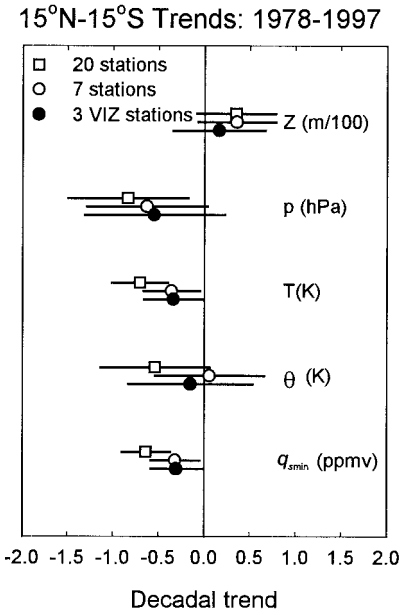

Figure 20. Trends in four different characteristics of the lapse-rate tropopause, and in minimum water vapor saturation volume mixing ratio, for 1978–1997, for the region 15°N–15°S. For each variable, trends based on 20 stations, 7 stations, and 3 stations (as discussed in the text) are shown. Confidence intervals are ±2 standard deviations of the trend estimate, with the number of degrees of freedom reduced to account for lag-1 autocorrelation.

with lower saturation mixing ratio, in the Northern Hemisphere than in the Southern Hemisphere in the NH winter. In the NH summer the tropopause is higher and at lower pressure in the Southern Hemisphere, but it remains colder in the Northern Hemisphere. The longitudes of minimum temperature (and saturation mixing ratio) differ from the longitudes of maximum height and minimum pressure. The tropopause is highest and at lowest pressure in the region over northern South America and east of Central America during the NH winter, and over Africa during other months. However, it is coldest over the western tropical Pacific most of the year.

3. The 100 hPa level is a poor surrogate for the tropical tropopause. The 100 hPa height shows significantly less spatial and temporal variability than the heights of the LRT and CPT. In particular, the 100 hPa level lacks the seasonal variations of the tropopause and resides in the stratosphere during the NH summer and in the troposphere during the NH winter. Therefore it is warmer in the mean than in the LRT and CPT.

4. Water vapor saturation volume mixing ratios at the CPT and LRT are very close to the minimum values for a given profile ($q_{s\min}$). However, values at the 100 hPa level are 10–25% higher.

5. Comparison of our results with tropopause climatologies based on analyses or reanalysis [*Highwood and Hoskins*, 1998; *Hoinka*, 1998, 1999] suggests that the analyses depict the tropopause at lower elevation, and with less spatial structure, than the radiosonde data. This is probably due to the relatively poor vertical resolution of the analyses near the tropopause level. Comparison with an earlier climatology based on radiosonde data [*Makhover*, 1979] shows better agreement.

6. Based on correlations of detrended monthly anomaly time series analysis for the equatorial zone, we find associations between tropopause height and conditions in both the lower stratosphere (18 km level) and the troposphere, including the surface. The height of the tropopause reflects the temperature of the underlying troposphere, and it decreases with decreasing atmospheric stability, suggesting an indirect response to convection. A direct local response to convection was observed by *Johnson* [1986] during the winter MONEX experiment in Indonesia. Tropopause temperature, on the other hand, is significantly correlated only with the temperature and pressure of the lower stratosphere, showing evidence of the quasi-biennial oscillation and the warming following the eruption of the El Chichón volcano.

7. The utility of the radiosonde data for detection of trends in the tropopause is limited by changes in instrumentation and observing methods. Taking these into account, we find some evidence for the following (nonmonotonic) trends in the tropopause in the deep tropics (15°N–15°S) during the period 1978–1997: an increase in height of about 20 m decade^{-1}, a decrease in pressure of about 0.5 hPa decade^{-1}, a cooling of about 0.5 K decade^{-1}, little change in potential temperature, and a decrease in water vapor saturation mixing ratio of about 0.3 ppmv decade^{-1}.

We hope that the data set presented here will be useful in other studies of the tropical tropopause, such as comparisons with model simulations and process studies. The data are available at Stratospheric Processes and Their Role in Climate (SPARC) Data Center (www.sparc.sunysb.edu), or by contacting the authors.

Acknowledgments. We thank Andrew Dessler (NASA and Univ. of Maryland), James Holton (Univ. of Washington), George Kiladis (NOAA Aeronomy Laboratory), Daniel Kirk-Davidoff (Harvard Univ.), Stephen Klein (NOAA Geophysical Fluid Dynamics Laboratory), XueLong Zhou (University of Washington), and an anonymous reviewer for providing helpful comments on this paper.

References

Angell, J. K., and J. Korshover, Quasi-biennial variations in temperature, total ozone, and tropopause height, *J. Atmos. Sci*., *21*, 479–492, 1964.

Angell, J. K., and J. Korshover, Quasi-biennial and long-term fluctuations in tropopause pressure and temperature, and the relation to stratospheric water vapor, *Mon. Weather Rev*., *102*, 29–34, 1974.

Angell, J. K., and J. Korshover, The relation between equatorial tropopause temperature and water vapor mixing ratio in the low stratosphere at Washington, D.C., *Mon. Weather Rev*., *104*, 756–760, 1976.

Brasseur, G., *The Stratosphere and Its Role in the Climate System*, *NATO ASI Ser*., vol. 54, Springer-Verlag, New York, 1997.

Dessler, A. E., A reexamination of the "stratospheric fountain" hypothesis, *Geophys. Res. Lett*., *25*, 4165–4168, 1998.

Dessler, A. E., E. J. Hintsa, E. M. Weinstock, J. G. Anderson, and K. R. Chan, Mechanisms controlling water vapor in the lower stratosphere: "A tale of two stratospheres," *J. Geophys. Res*., *100*, 167–23,172, 1995.

Eskridge, R. E., O. A. Alduchov, I. V. Chernykh, Z. Panmao, A. C. Polansky, and S. R. Doty, A Comprehensive Aerological Reference Data Set (CARDS): Rough and systematic errors, *Bull. Am. Meteorol. Soc*., *76*, 1759–1775, 1995.

Evans, J. S., R. Toumi, J. E. Harries, M. P. Chipperfield, and J. R. Russell III, Trends in stratospheric humidity and the sensitivity of ozone to those trends, *J. Geophys. Res*., *103*, 8715–8725, 1998.

Forster, P. M. de F., and K. P. Shine, Stratospheric water vapour changes as a possible contributor to observed stratospheric cooling, *Geophys. Res. Lett*., *26*, 3309–3312, 1999.

Frederick, J. E., and A. R. Douglass, Atmospheric temperatures near the tropical tropopause: Temporal variations, zonal asymmetry and implications for stratospheric water vapor, *Mon. Weather Rev*., *111*, 1397–1403, 1983.

Gaffen, D. J., Temporal inhomogeneities in radiosonde temperature records, *J. Geophys. Res*., *99*, 3667–3676, 1994.

Gaffen, D. J., B. D. Santer, J. S. Boyle, J. R. Christy, N. E. Graham, and R. J. Ross, Multi-decadal changes in the vertical temperature structure of the tropical troposphere, *Science*, *287*, 1239–1241, 2000a.

Gaffen, D. J., M. A. Sargent, R. E. Habermann, and J. R. Lanzante, Sensitivity of tropospheric and stratospheric temperature trends to radiosonde data quality, *J. Clim*., *13*, 1776–1796, 2000b.

Gage, K. S., and G. C. Reid, Response of the tropical tropopause to El Chichón and the El Niño of 1982–83, *Geophys. Res. Lett*., *12*, 195–197, 1985.

Gage, K. S., and G. C. Reid, Longitudinal variations in the tropical tropopause properties in relation to tropical convection and El Niño-Southern Oscillation events, *J. Geophys. Res*., *92*, 14,197–14,203, 1987.

Gibson, J. K., P. Kållberg, S. Uppala, A. Hernandez, A. Nomura, and E. Serrano, *ERA Description, ECMWF Reanal. Proj. Rep. Ser*., vol. 1, 66 pp., Eur. Cent. for Medium-Range Weather Forecasts, Reading, England, 1997.

Highwood, E. J., and B. J. Hoskins, The tropical tropopause, *Q. J. R. Meteorol. Soc*., *124*, 1579–1604, 1998.

Hoinka, K. P., The tropopause; discovery, definition and demarcation, *Meteorol. Z*., *6*, 281–303, 1997.

Hoinka, K. P., Statistics of the global tropopause pressure, *Mon. Weather Rev*., *126*, 3303–3325, 1998.

Hoinka, K. P., Temperature, humidity, and wind at the global tropopause, *Mon. Weather Rev*., *127*, 2248–2265, 1999.

Holton, J. R., P. H. Haynes, M. E. McIntyre, A. R. Douglass, R. B. Rood, and L. Pfister, Stratosphere-troposphere exchange, *Rev. Geophys*., *33*, 403–439, 1995.

Johnson, R. H., Short-term variations of the tropopause height over the winter MONEX area, *J. Atmos. Sci*., *43*, 1152–1163, 1986.

Kalnay, E., et al., The NCEP/NCAR 40-year reanalysis project, *Bull. Am. Meteorol. Soc*., *77*, 437–471, 1996.

Kirk-Davidoff, D. B., E. J. Hinsta, J. G. Anderson, and D. W. Keith, The effect of climate change on ozone depletion through changes in stratospheric water vapour, *Nature*, *202*, 399–401, 1999.

Luers, J. K., and R. E. Eskridge, Use of radiosonde temperature data in climate studies, *J. Clim*., *11*, 1002–1019, 1998.

Makhover, Z. M., Features of the tropopause distribution over the globe (in Russian), *Meteorol. Geophys*., *12*, 33–39, 1979.

Mote, P. W., K. H. Rosenlof, M. E. McIntyre, E. S. Carr, J. C. Gille, J. R. Holton, J. S. Kinnersley, H. C. Pumphrey, J. M. Russell III, and J. W. Waters, An atmospheric tape recorder: The imprint of tropical tropopause temperatures on stratospheric water vapor, *J. Geophys. Res*., *101*, 3989–4006, 1996.

Nedoluha, G. E., R. M. Bevilacqua, R. M. Gomez, D. E. Siskind, B. C. Hicks, J. M. Russell III, and B. J. Conner, Increases in middle atmospheric water vapor as observed by the Halogen Occultation Experiment and the ground-based water vapor millimeter-wave spectrometer from 1991 to 1997, *J. Geophys. Res*., *103*, 3531–3543, 1998.

Newell, R. E., and S. Gould-Stewart, A stratospheric fountain? *J. Atmos. Sci*., *38*, 2789–2796, 1981.

Ohring, G., A most surprising discovery, *Bull. Am. Meteorol. Soc*., *45*, 12–14, 1964.

Oltmans, S. J., and D. J. Hofmann, Increase in lower-stratospheric water vapour at a mid-latitude Northern Hemisphere site from 1981 to 1994, *Nature*, *374*, 146–149, 1995.

Parker, D. E., M. Gordon, D. P. N. Cullum, D. M. H. Sexton, C. K. Folland, and N. Rayner, A new global gridded radiosonde temperature database and recent temperature trends, *Geophys. Res. Lett*., *24*, 1499–1502, 1997.

Pawson, S., and M. Fiorino, A comparison of reanalyses in the tropical stratosphere, part 1, Thermal structure and the annual cycle, *Clim. Dyn*., *14*, 631–644, 1998.

Randel, W. J., F. Wu, and D. J. Gaffen, Interannual variability of the tropical tropopause derived from radiosonde data and NCEP reanalyses, *J. Geophys. Res*., *105*, 15,509–15,524, 2000.

Reed, R. J., A study of a characteristic type of upper level frontogenesis, *J. Meteorol*., *12*, 226–237, 1955.

Reid, G. C., and K. S. Gage, On the annual variation in height of the tropical tropopause, *J. Atmos. Sci*., *38*, 1928–1938, 1981.

Reid, G. C., and K. S. Gage, A relationship between the height of the tropical tropopause and the global angular momentum of the atmosphere, *Geophys. Res. Lett*., *1*, 840–842, 1984.

Reid, G. C., and K. S. Gage, Interannual variations in the height of the tropical tropopause, *J. Geophys. Res*., *90*, 5629–5635, 1985.

Reid, G. C., and K. S. Gage, The tropical tropopause over the western Pacific: Wave driving, convection, and the annual cycle, *J. Geophys. Res*., *101*, 21,233–21,241, 1996.

Rosenlof, K. H., Seasonal cycle of the residual mean meridional circulation in the stratosphere, *J. Geophys. Res*., *100*, 5173–5192, 1995.

Shimizu, A., and T. Tsuda, Variations in tropical tropopause observed with radiosondes in Indonesia, *Geophys. Res. Lett*., *27*, 2541–2544, 2000.

Simmons, A. J., A. Untch, C. Jakob, P. Kållberg, and P. Undén, Stratospheric water vapour and tropical tropopause temperatures in ECMWF analyses and multi-year simulations, *Q. J. R. Meteorol. Soc*., *125*, 353–386, 1999.

Steinbrecht, W., H. Claude, U. Kohler, and K. P. Hoinka, Correlations between tropopause height and total ozone: Implications for long-term changes, *J. Geophys. Res*., *103*, 19,183–19,192, 1998.

Thuburn, J., and G. C. Craig, GCM tests of theories for the height of the tropopause, *J. Atmos. Sci*., *54*, 869–882, 1997.

Thuburn, J., and G. C. Craig, Stratospheric influence on tropopause height: The radiative constraint, *J. Atmos. Sci*., *57*, 17–28, 2000.

Vömel, H., and S. J. Oltmans, Comment on "A reexamination of the 'stratospheric fountain' hypothesis" by A. E. Dessler, *Geophys. Res. Lett*., *26*, 2737–2738, 1999.

Wallis, T. W. R., A subset of core stations from the Comprehensive Aerological Reference Dataset (CARDS), *J. Clim*., *11*, 272–282, 1998.

WMO, Meteorology—A three-dimensional science: Second session of the commission for aerology, *WMO Bull*., *IV*(4), 134–138, 1957.

WMO, *Guide to Meteorological Instruments and Methods of Observation*, 6th ed., *WMO Rep. 8*, World Meteorol. Organ., Geneva, Switzerland, 1996.

Zhou, X. L., M. A. Geller, and M. Zhang, Tropical cold point tropopause characteristics derived from reanalyses and soundings, *J. Clim*., in press, 2000.

Zhou, X. L., M. A. Geller, and M. Zhang, Cooling trend of the tropical cold point tropopause temperatures and its implications, *J. Geophys. Res*., *106*, 1511–1522, 2001.

J. K. Angell, R. J. Ross, and D. J. Seidel, NOAA Air Resources Laboratory (R/ARL), 1315 East West Highway, Silver Spring, MD 20910. (dian.seidel@noaa.gov)

G. C. Reid, Cooperative Institute for Research in Environmental Sciences, University of Colorado, Boulder, CO 80309.

(Received July 21, 2000; revised November 17, 2000;
accepted November 25, 2000.)